Photocatalysts

International Edition: DOI: 10.1002/anie.201501788
German Edition: DOI: 10.1002/ange.201501788

# Graphitic Carbon Nitride Polymers toward Sustainable Photoredox Catalysis

*Yun Zheng, Lihua Lin, Bo Wang, and Xinchen Wang**

**Keywords:**
conjugated polymer · graphitic carbon nitride · photocatalysis · two-dimensional materials · water splitting

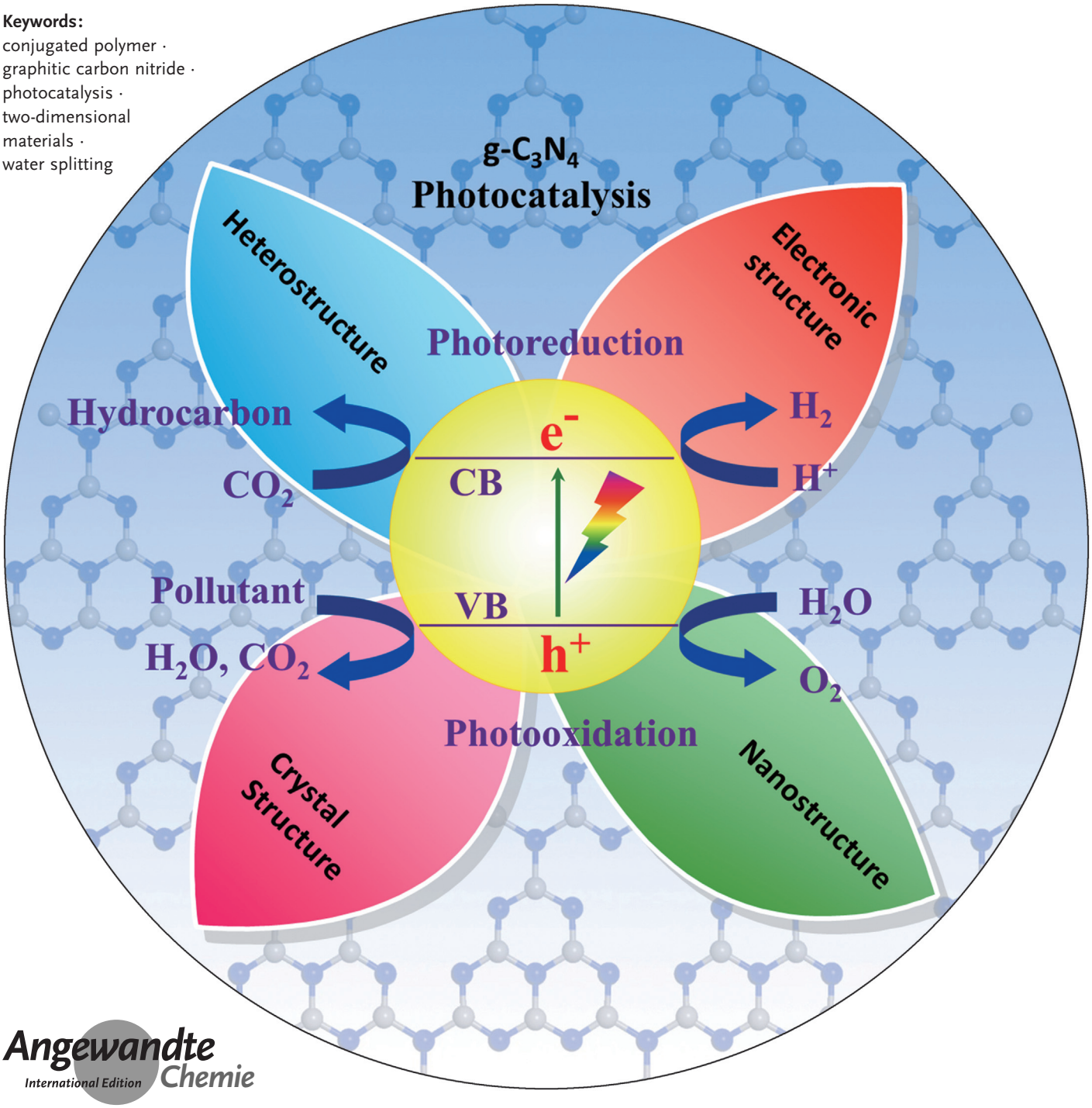

*As a promising two-dimensional conjugated polymer, graphitic carbon nitride (g-$C_3N_4$) has been utilized as a low-cost, robust, metal-free, and visible-light-active photocatalyst in the field of solar energy conversion. This Review mainly describes the latest advances in g-$C_3N_4$ photocatalysts for water splitting. Their application in $CO_2$ conversion, organosynthesis, and environmental purification is also briefly discussed. The methods to modify the electronic structure, nanostructure, crystal structure, and heterostructure of g-$C_3N_4$, together with correlations between its structure and performance are illustrated. Perspectives on the challenges and opportunities for the future exploration of g-$C_3N_4$ photocatalysts are provided. This Review will promote the utilization of g-$C_3N_4$ materials in the fields of photocatalysis, energy conversion, environmental remediation, and sensors.*

**From the Contents**



## 1. Introduction

The photocatalytic production of hydrogen fuel and chemicals by using $CO_2$ and $H_2O$ as the raw materials has been a relevant and active research topic for the past 40 years, as inspired by plant photosynthesis (Figure 1). Since the landmark event of photoelectrochemical splitting of water on

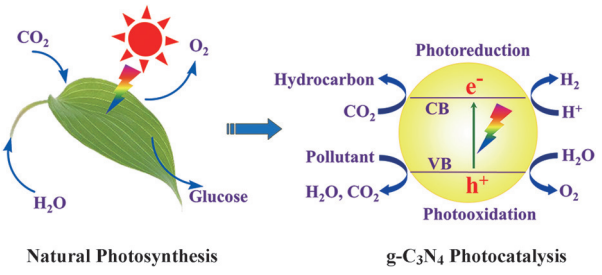


***Figure 1.*** Natural photosynthesis and the photocatalytic process of g-$C_3N_4$. Reproduced from Ref. [2a] with permission. Copyright 2013, Elsevier.

n-type $TiO_2$ electrodes in 1972, photocatalytic technology has been considered one of the most important approaches to address global energy and environmental issues.[1] To date, research has mainly focused on the development of metal-based oxides, sulfides, nitrides, and phosphides, as well as their mixed solid solutions as inorganic solar energy transducers to generate energized electrons and holes to induce chemical reactions.[2]

The discovery of the graphitic carbon nitride polymer as a metal-free, two-dimensional conjugated semiconductor has stimulated intensive research in sustainable photocatalysis with conjugated polymers for water splitting since 2009 (Figure 1), potentially shifting the search for photocatalysts from inorganic semiconductors to more abundant organic/polymeric ones.[3] However, the photocatalytic activity of pristine g-$C_3N_4$ (quantum efficiency = 0.1 % at 420–460 nm) is still low because of the small specific surface area, marginal optical absorption in the visible region, fast rate of charge recombination, and low electric conductivity.[4]

The photocatalytic activities of g-$C_3N_4$ are greatly influenced by the structure,[5] including the electronic structure, nanostructure, crystal structure, and/or heterostructure. In recent years, many synthetic techniques and effective modification procedures to optimize the photoactivity of g-$C_3N_4$ from the perspectives of electronic structure modulation, nanostructure design, crystal structure engineering, and heterostructure construction have been proposed. Doping and copolymerization have both been demonstrated to be efficient to incorporate external impurities into g-$C_3N_4$ to modulate its electronic structure and photocatalytic performance. With regard to nanostructure design, nanostructures with controllable morphologies not only facilitate mass transfer in catalysis but also accelerate the collection and separation of electron–hole pairs to drive relevant reactions.[6] A series of g-$C_3N_4$ materials with nanopores and nanoscale geometrical shapes have been developed by a variety of synthetic pathways, including hard/soft templating strategies, supramolecular preorganization, solvothermal technology, and exfoliation strategies. With respect to crystal-structure engineering, ionothermal synthesis opens up great opportunities for the synthesis of highly crystalline, more completely condensed g-$C_3N_4$ with enhanced photocatalytic activity.[7] The synthesis of heterostructured composites by coupling g-$C_3N_4$ with other semiconductors not only suppresses the recombination of photoinduced charge, but also endows the composites with enhanced properties or novel features as a result of the synergistic effects.[8] Therefore, the rational design of the structure at different levels would provide new

[*] Y. Zheng, L. Lin, B. Wang, Prof. X. Wang
State Key Laboratory of Photocatalysis on Energy and Environment
College of Chemistry, Fuzhou University
Fuzhou 350002 (China)
E-mail: xcwang@fzu.edu.cn
Homepage: http://wanglab.fzu.edu.cn

  

insights to create high-performance g-$C_3N_4$ materials for the efficient conversion of solar energy.

There is a rapidly growing collection of publications concerning basic and applied studies on the synthesis and modification of g-$C_3N_4$ for sustainable photoredox catalysis. Approximately 800 publications can be found by searching the *Web of Science* with the keywords "carbon nitride" and "photocataly*", with more than 7000 cross-citations in 2014 alone. Some recent reviews have been published on the history, structure, synthesis, properties, and applications of g-$C_3N_4$.[9] However, thus far, a comprehensive review on the latest progress is still lacking. In this Review, we mainly overview the advances made in the use of g-$C_3N_4$ for photocatalytic splitting of water, and briefly introduce the application of g-$C_3N_4$ photocatalysts in other fields. The methods for modifying the electronic structure, nanostructure, crystal structure, and heterostructure of g-$C_3N_4$ are discussed. Moreover, the effect of structure on the properties and photocatalytic activities of g-$C_3N_4$ are demonstrated. Finally, the opportunities and challenges in this field are discussed. This Review aims to promote the further development of g-$C_3N_4$ polymers as a new generation of functional nanomaterials in the fields of energy conversion, environmental remediation, catalysis, sensor design, and sustainable chemistry.

## 2. Photocatalysis with Graphitic Carbon Nitride

$C_3N_4$ represents a class of the oldest synthetic polymers that consist mainly of carbon and nitrogen. The history of carbon nitride polymers and their precursors can be traced back to 1834, when a polymeric derivative was made by Berzelius and termed "melon" by Liebig.[10]

There are seven phases of $C_3N_4$, that is, α-$C_3N_4$, β-$C_3N_4$, cubic $C_3N_4$, pseudocubic $C_3N_4$, g-h-triazine, g-o-triazine, and g-h-heptazine, with band gaps of 5.49, 4.85, 4.30, 4.13, 2.97, 0.93, and 2.88 eV, respectively.[11] Both triazine ($C_3N_3$) and tri-*s*-triazine/heptazine ($C_6N_7$) rings were discussed as basic tectonic units to constitute potential allotropes of g-$C_3N_4$ (Figure 2). Tri-*s*-triazine-based g-$C_3N_4$ was found to be energetically favored relative to the other phases and was considered the most stable phase of $C_3N_4$ under ambient conditions.[11] Only the pseudocubic and g-h-triazine phases have direct band gaps; all of the other phases have indirect band gaps in their bulk structures.[11] Based on the band gap energies, both the g-h-heptazine and g-h-triazine phases are suitable for the photocatalytic production of $H_2$.[11]

A new avenue of g-$C_3N_4$ photocatalysis was opened up in 2009. It was reported that a g-$C_3N_4$ polymer exhibits photocatalytic activity for water splitting in the presence of a proper sacrificial electron donor or acceptor, even in the absence of co-catalysts.[3a] Density functional theory (DFT) calculations were performed to gain insight into the electronic structure of g-$C_3N_4$ (Figure 3).[3a] The investigation revealed that the valence and conduction bands are mainly composed of the nitrogen $p_z$ orbitals and carbon $p_z$ orbitals, respectively.[3a] The light-trigged electrons and holes indicate that oxidation and reduction sites for splitting water occur independently in the nitrogen atoms and carbon atoms.[3a] There are many advantages of g-$C_3N_4$ photocatalysts for water splitting: 1) The band gap of 2.7 eV is sufficiently large to overcome the endothermic character of the water-splitting reaction, and the optical absorption edge of 460 nm allows the possibility to harness visible light.[3a,12] 2) The electronic bands of g-$C_3N_4$

*Yun Zheng obtained her BS in chemistry from Fuzhou University (2012), P.R. China. She is now pursing her PhD in Prof. Xinchen Wang's group at State Key Laboratory of Photocatalysis on Energy and Environment, College of Chemistry, Fuzhou University, P.R. China. Her main research interest is the synthesis of nanostructured graphitic carbon nitrides.*

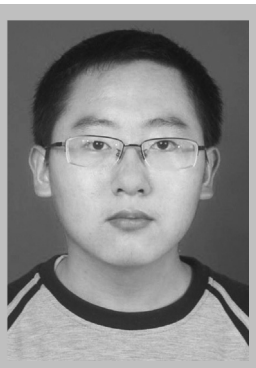

*Bo Wang obtained his BS in chemistry from Fuzhou University (2013), P.R. China. He is now pursing his PhD under the supervision of Prof. Xinchen Wang at the State Key Laboratory of Photocatalysis on Energy and Environment, College of Chemistry, Fuzhou University, P.R. China. His main research interest is the fabrication of nanostructured graphitic carbon nitrides and their applications in artificial photosynthesis.*

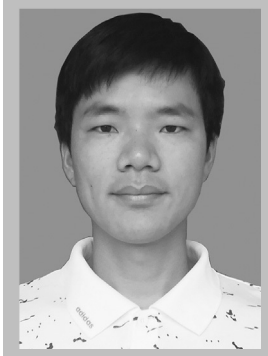

*Lihua Lin received his BS in physics from Harbin University (2009). He is currently a PhD student supervised by Prof. Xinchen Wang at State Key Laboratory of Photocatalysis on Energy and Environment, College of Chemistry, Fuzhou University, P.R. China. His research focuses on the utilization of solar energy and graphitic carbon nitride materials for solar production of hydrogen.*

*Xinchen Wang obtained his BS from Fuzhou University and his PhD from The Chinese University of Hong Kong. He was then a postdoctoral fellow at Tokyo University and an Alexander von Humboldt Fellow and a Group Leader at the Max Planck Institute of Colloids and Interfaces, Germany. He is currently a professor at State Key Laboratory of Photocatalysis on Energy and Environment, College of Chemistry, Fuzhou University, P.R. China. His research concerns designing solar energy materials for water splitting, $CO_2$ fixation, and organocatalysis with sunlight.*

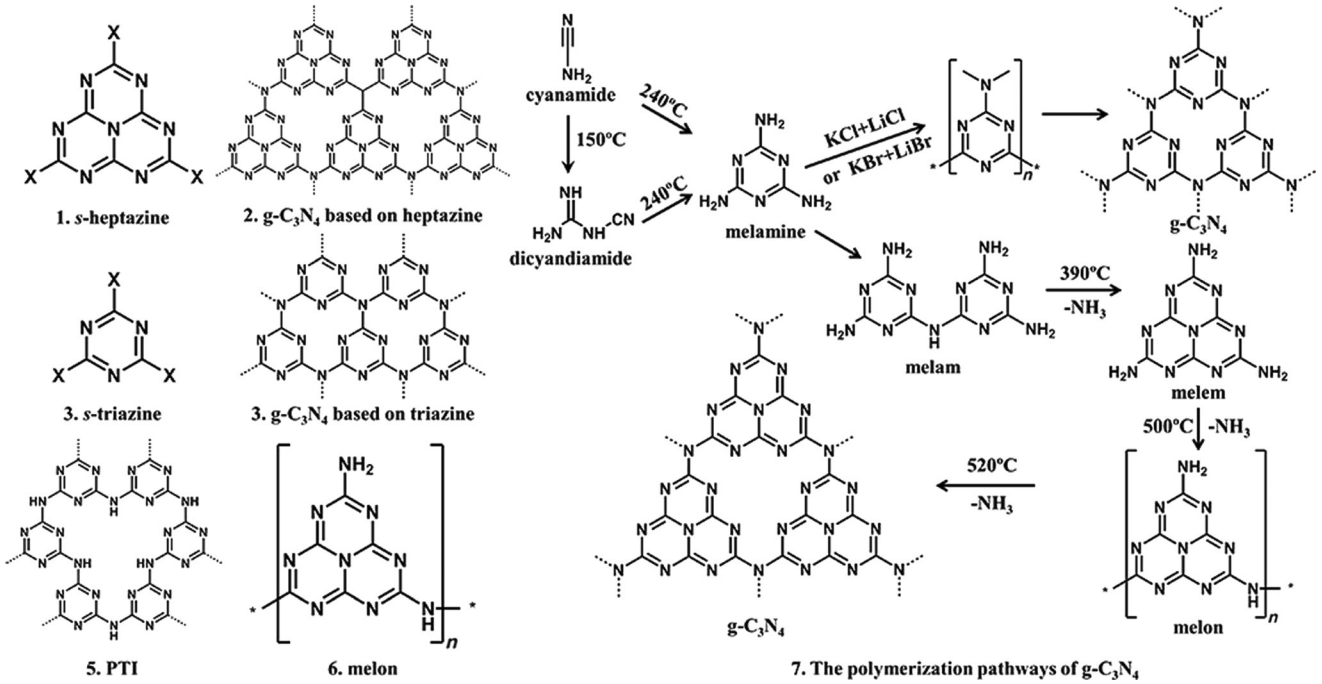


***Figure 2.*** Left: structures of *s*-heptazine, *s*-triazine, hypothetical g-$C_3N_4$, poly(triazine imide) (PTI), and melon. Right: Thermal polymerization pathways of g-$C_3N_4$.

cover the redox potentials of water; thus, the photogenerated electron is sufficiently reductive to reduce water to $H_2$, and the photogenerated hole has sufficient oxidation power to oxidize water to liberate $O_2$.[3a,12] 3) g-$C_3N_4$ is chemically and thermally stable and is not subject to photocorrosion in the water-splitting reaction, unlike other conductive polymers.[3a,12] 4) g-$C_3N_4$ has a specific microstructure, with surface termination as defects and nitrogen atoms for electron localization or anchoring inorganic/organic functional motifs as the active sites.[3a,12] Thus, g-$C_3N_4$ is regarded as a promising metal-free photocatalyst that offers new opportunities in the field of artificial photosynthesis.

Nitrogen-rich and oxygen-free compounds containing C-N core structures (e.g. cyanamide, dicyandiamide, and melamine) are widely used as the precursors to synthesize g-$C_3N_4$.[9a] The thermal condensation of cyanamide to dicyandiamide and then to melamine has been recognized as a facile synthetic pathway to generate the g-$C_3N_4$ polymer.[7a,13] The intermediate steps along the thermal condensation of the molecular precursors are shown schematically in Figure 2.[7a,13]

The reaction is an integration of a polyaddition and polycondensation process where the precursors are first condensed to melamine. The second step is a condensation process in which ammonia is eliminated; thus, the products differ when performed in closed and open reaction flasks. Melamine-based products are typically present above 350 °C, whereas the tri-*s*-triazine products are obtained from rearrangements of melamine at approximately 390 °C. The condensation of this unit to polymers, networks, and the final polymeric $C_3N_4$ occurs at approximately 520 °C. The material becomes slightly unstable above 600 °C. Heating to 700 °C results in the generation of nitrogen and cyano fragments and the residue-free disappearance of the material. However, g-$C_3N_4$ solids obtained from the thermal condensation of monomers were not perfectly crystalline and have a C/N molar ratio of approximately 0.72:1 and a small amount of H (ca. 2 wt.%), close to the structure of the "melon" polymer featuring hydrogen.[9b]

## 3. Electronic Structure Modulation

The electronic structure and energy-band configuration of a semiconductor play a key role in determining the absorption of light and the redox potentials.[14] Considering the polymeric nature of g-$C_3N_4$ and an ample choice of precursors, dopants, and co-monomers, modulation of the electronic structure represents an effective approach to the exploration and development of visible-light-sensitive g-$C_3N_4$ photocatalysts with optimized performance.

### 3.1. Doping

Doping, a process of incorporating external impurities into a semiconductor, is widely used as an essential method to modulate the electronic structure of semiconductors for the manipulation of conductive, optical, luminescent, magnetic, or other physical properties.[15] In photocatalysis, band-gap engineering through the addition of cations, anions, or their cooperative doping has been demonstrated as an effective procedure to modify g-$C_3N_4$ photocatalysts for targeted solar energy applications.

Many anions, including B, F, C, O, P, S, and I, have been incorporated into g-$C_3N_4$.[16] Sulfur-doped g-$C_3N_4$, which was

  

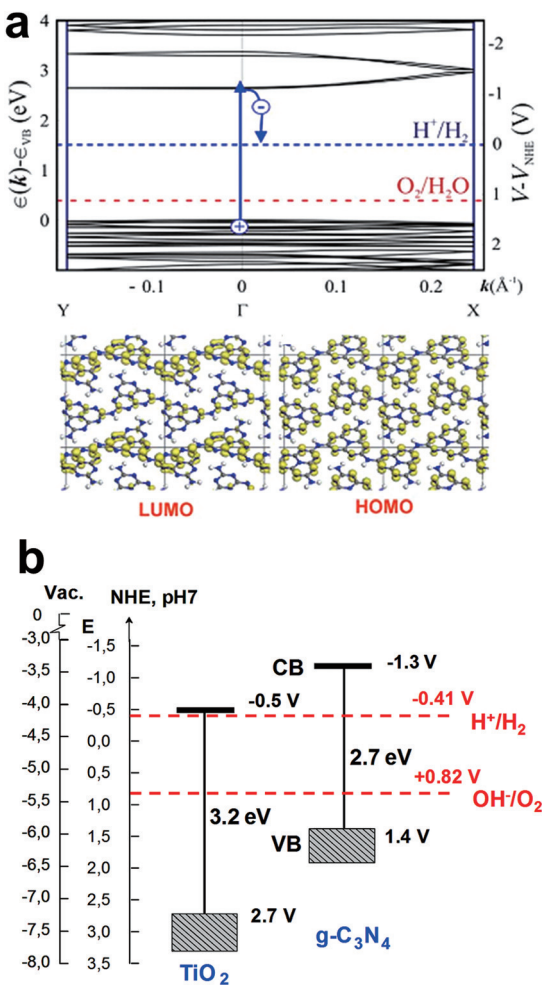


***Figure 3.*** a) Electronic structure of the polymeric melon. Reproduced from Ref. [3a] with permission. Copyright 2008, Nature Publishing Group. b) Electronic band structure of g-$C_3N_4$ and titanium oxide ($TiO_2$). Reproduced from Ref. [12] with permission. Copyright 2012, Royal Society of Chemistry.

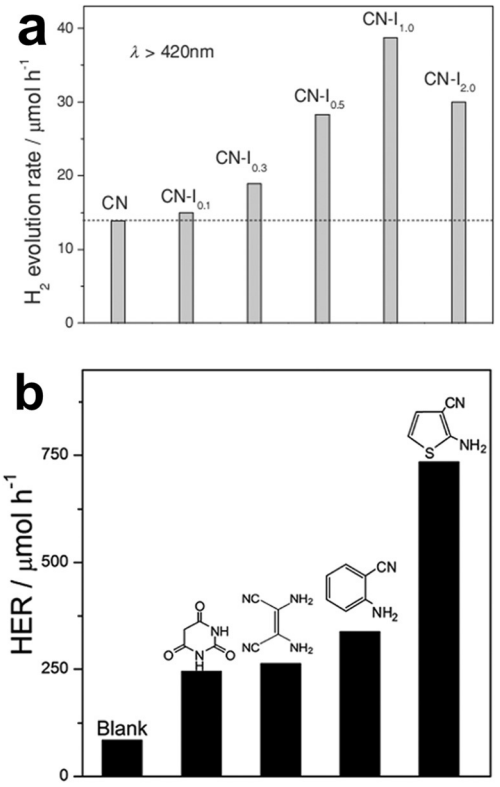


***Figure 4.*** a) Photocatalytic $H_2$ evolution rate (HER) for different iodine-doped CN-Ix samples with visible light. Reproduced from Ref. [17] with permission. Copyright 2014, Wiley-VCH. b) HER of g-$C_3N_4$ synthesized by copolymerization of urea with different monomers, using 3 wt% Pt as co-catalyst. Reproduced from Ref. [24] with permission. Copyright 2014, the Royal Society of Chemistry.

fabricated by the thermal treatment of g-$C_3N_4$ under a $H_2S$ atmosphere, features an electronic structure with an enlarged valence bandwidth, an elevated conduction band minimum, and a slightly diminished absorbance.[16d] These characteristics lead to a distinctive electronic structure that efficiently enhances the photoreduction reactivity in the evolution of $H_2$.[16d] The use of trithiocyanuric acid as the precursor, where the -SH groups act as the leaving groups during polycondensation, led to the resultant $CNS_{600}$ having a more stable structure; the valance band (VB) is lowered by about 0.2 V, while still possessing sufficient potential for the reduction of water.[3b] Thus, the $CNS_{600}$ samples exhibited a significant improvement in the activity of $H_2$ evolution over g-$C_3N_4$, with stable $O_2$ evolution under irradiation with light.[3b] Our group reported that iodine-functionalized g-$C_3N_4$ effectively modifies its semiconductive, textural, and photocatalytic properties (Figure 4a).[17] The modification with iodine endows g-$C_3N_4$ with an enhanced optical absorption, an enlarged surface area, an accelerated charge-transfer rate, and an increased rate of $H_2$ evolution.[17]

In addition, various metal cations (e.g. Fe, Mn, Co, Ni, Cu, Zn, Ag, Eu, and Pd) have been doped into g-$C_3N_4$.[18] The incorporation of appropriate amounts of $Fe^{3+}$ ions into a g-$C_3N_4$ matrix strongly modifies the electronic properties of g-$C_3N_4$ and provides the material with increased photocatalytic reactivity for the degradation of rhodamine B by $H_2O_2$.[18a] Doping with different cation species also affects the photocatalytic application and activity of the resultant catalysts. For example, Fe-g-$C_3N_4$/SBA-15 was found to be active for the hydroxylation of benzene to phenol with $H_2O_2$, whereas Co-g-$C_3N_4$ exhibits a good catalytic performance for the epoxidation of styrene with $O_2$.[18b] Dual doping has a stronger influence on the photocatalytic reactivity than doping with a single heteroatom. g-$C_3N_4$ co-doped with Fe and P exhibited a higher photocatalytic activity than single-doped and undoped g-$C_3N_4$ catalysts.[19] The addition of dopants inhibited the crystal growth of g-$C_3N_4$, enhanced the surface area, decreased the band gap energy, and restrained the recombination of charge carriers.[19] However, the doping strategy may also have some unfavorable effects, such as creating more defects for the recombination of photogenerated carriers because of doping asymmetry and impurities.[20]

### 3.2. Copolymerization

The photocatalytic properties of bulk g-$C_3N_4$ originate from its π-conjugated system as a result of the $sp^2$ hybridization of C and N; therefore, it is desirable to extend the delocalization of the π electrons and to change the intrinsic semiconductor properties by grafting aromatic groups onto the surface of g-$C_3N_4$.[21] This copolymerization is a form of molecular doping and is a good candidate to modulate the π electrons of the g-$C_3N_4$ aromatic system, band structure, and photoactivity.[21]

Enhancement of the photocatalytic performance was first demonstrated by copolymerizing barbituric acid with the g-$C_3N_4$ precursor through a Schiff base reaction. The enhancement results from the extension of the optical absorption of the polymer to cover more of the visible range.[21] However, in this case, the HOMO was decreased in energy, thus lowering the oxidation potential, which is presumably the most difficult step in achieving overall water splitting with organic semiconductors.[21] The design of appropriate co-monomers with diverse chemical composition and structure allows for the modification of the band structure and optoelectronic properties of g-$C_3N_4$.[21] As most precursors of g-$C_3N_4$ contain cyano groups and/or amino groups,[9a,22] this strategy was further advanced by employing a variety of new monomers as building blocks with the desired compositions and electronic structures for chemical incorporation into the g-$C_3N_4$ network.[21] The bottom-up synthesis of g-$C_3N_4$ for photocatalysis with visible light is achieved by the polymerization of dicyandiamide or urea with organic monomers bearing cyano groups and/or amino groups.[23,24] This design allows ample choice of organic anchoring groups (e.g. benzene, pyridine, thiophene, and diaminomaleodinitrile) and is potentially valuable to alter the physical and chemical properties of the resulting heterogeneous organocatalysts.[23,24] Low-dimensional g-$C_3N_4$ nanosheets were synthesized for the photocatalytic splitting of water by the one-pot condensation of urea with organic co-monomers.[24] Such a condensation brings about a red-shift of the optical absorption, improved charge separation, and a high quantum efficiency of 8.8% at 420 nm for $H_2$ generation (Figure 4b).[24] The incorporation of electron-rich thiophene moieties in the conjugated polymer can effectively change the intrinsic bulk and surface features of g-$C_3N_4$, such as engineering the electronic structure with a tunable band gap and promoting the charge-carrier migration and separation through the formation of surface dyadic structures, thus leading to an increase in the photocatalytic activity for $H_2$ generation.[25] In comparison, the position of the valance band can be greatly decreased by incorporating the electron-deficient pyromellitic dianhydride (PMDA) monomer into the network of g-$C_3N_4$, thereby providing a strong photooxidation capability.[26] The modified photocatalyst exhibits preferential activity for water oxidation over water reduction compared to g-$C_3N_4$.[26] Strikingly, the active species involved in the photodegradation of methyl orange switches from photogenerated electrons to holes after engineering of the band structure.[26]

Moreover, by combining copolymerization and nanostructure design, a mesoporous g-$C_3N_4$ with an integrated thiophene motif (MCN-ATCN) was constructed by the reaction of dicyandiamide with different amounts of 3-aminothiophene-2-carbonitrile (ATCN) and template synthesis using 12 nm silica nanoparticles.[27] MCN-ATCN exhibits a modified aromatic π-conjugated system, improved semiconductor properties, and enhanced reactivity for the photoactivation of oxygen for the selective oxidation of aromatic alcohols.[27]

These studies may provide guidance for designing efficient polymer photocatalysts with desirable chemical compositions and electronic structures for specific photoreactions.[26]

## 4. Nanostructure Design

The emergence of nanostructured semiconductors as photocatalysts has contributed to diverse and flexible pathways to improve photocatalytic efficiency.[14] Notable progress has been achieved in the shape-controlled preparation of g-$C_3N_4$ and in investigations of the relationship between the morphological features and the photocatalytic activities in recent years. The synthesis of g-$C_3N_4$ nanomaterials can be divided into two categories: "top down" and "bottom up."[28] The top-down approach tends to cut larger, externally controlled components into subunits, whereas the bottom-up approach seems to have smaller components that are built up into complex structures. With respect to the manufacture of g-$C_3N_4$ nanomaterials, the former approach is mainly based on liquid or thermal exfoliation methods, and the latter primarily includes the template method, supramolecular preorganization, and solvothermal synthesis.

### 4.1. Top-Down Strategy

As the thinnest functional nanomaterials, two-dimensional (2D) g-$C_3N_4$ nanosheets with atomic or molecular thickness, infinite planar lengths, and a large surface area exhibit outstanding optical, electrical, thermal, and mechanical properties and thereby have a broad application potential in energy conversion, optoelectronics, catalysis, sensing, and biotechnology.[29] A top-down approach is utilized to break the g-$C_3N_4$ block system down to its compositional subsystems, namely, g-$C_3N_4$ nanosheets. Single- or few-layer g-$C_3N_4$ nanosheets could be obtained using top-down strategies, including liquid exfoliation, liquid ammonia assisted lithiation, and thermal exfoliation methods.

The liquid exfoliation method is widely used for the synthesis of g-$C_3N_4$ nanosheets. A variety of monolayer or multilayer g-$C_3N_4$ nanosheets have been successfully extracted by a liquid exfoliation method from g-$C_3N_4$ powder in certain solvents (such as water,[30] 2-propanol,[31] 1,3-butanediol,[32] water/2-propanol,[33] and 2-propanol/dimethyl formamide/water)[34] by sonication. Xie and coworkers prepared g-$C_3N_4$ nanosheets by a liquid exfoliation route from bulk g-$C_3N_4$ in water.[30] The nanosheets exhibit a size distribution ranging from 70 to 160 nm and a height of 2.5 nm, which corresponds to about 7 atomic layers (Figure 5a).[30] Compared with bulk g-$C_3N_4$, the nanosheets

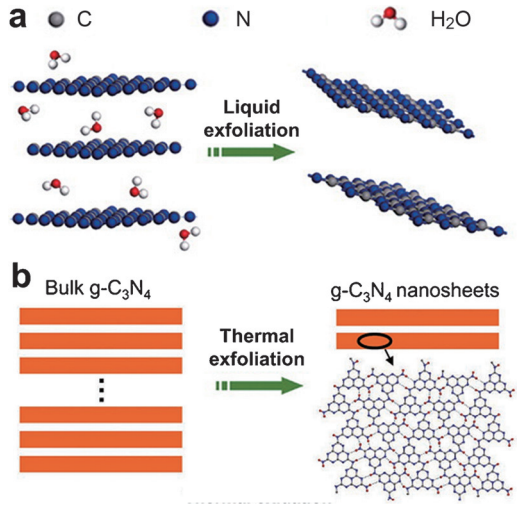


***Figure 5.*** a) Liquid exfoliation of bulk g-$C_3N_4$ to give nanosheets. Carbon, nitrogen, and hydrogen atoms are indicated by gray, blue, and red spheres, respectively, in the atomic model. Reproduced from Ref. [30] with permission. Copyright 2013, American Chemical Society. b) Thermal exfoliation of bulk g-$C_3N_4$ to nanosheets. Reproduced from Ref. [39a] with permission. Copyright 2012, Wiley-VCH.

exhibit an enhanced photoabsorption and photoresponse, which not only enhance the photocurrent and photocatalytic activity but also induce a high photoluminescence (PL) quantum yield up to 19.6%.[30] The water-soluble g-$C_3N_4$ nanosheet with its inherent blue light PL, high quantum yields, high stability, good biocompatibility, and nontoxicity is a new but promising candidate for both photocatalytic and bioimaging applications.[30] However, most of the as-prepared g-$C_3N_4$ nanosheets are composed of more than 6 layers and are more than 2 nm thick. Thus, preparing real graphene-like g-$C_3N_4$ with a single atomic layer remains challenging.[35] Zhu and co-workers reported that the ultrathin g-$C_3N_4$ nanosheets with a single atomic thickness of 0.4 nm were prepared by a chemical exfoliation method by mixing g-$C_3N_4$ with $H_2SO_4$ (98 wt%) before sonication in water.[36] Compared with the bulk g-$C_3N_4$, single-layer g-$C_3N_4$ nanosheets show great superiority in the transfer and separation of charge carriers.[36] Accordingly, the photocatalytic production of $H_2$, activities of pollutant decomposition, and photocurrent generation of single-layer g-$C_3N_4$ nanosheets are considerably higher than those of the bulk g-$C_3N_4$, thus indicating the great application potential of single-layer g-$C_3N_4$ nanosheets in photocatalysis.[36] However, 40% of the product still consists of multilayer nanosheets.[36] Quan and co-workers undertook a "bulk-nanosheet-single layer" route to prepare atomic single-layer g-$C_3N_4$ nanosheets with a thickness of 0.4–0.5 nm by an ultrasonic exfoliation process by employing few-layer g-$C_3N_4$ nanosheets as precursors.[37] During the photocatalytic process under irradiation with visible light, the degradation rate of rhodamine B on a single-layer g-$C_3N_4$ nanosheet was approximately 3.0- and 10.2-fold higher than that for the few-layer g-$C_3N_4$ nanosheets and bulk g-$C_3N_4$, respectively.[37] This high photocatalytic performance is attributed to the single-layer structure of the g-$C_3N_4$ nanosheets, which lengthens the lifetime of photogenerated charges and serves as an excellent electron transporter.[37] Wu and co-workers developed a versatile and scalable mixed-solvent strategy for the liquid exfoliation of bulk g-$C_3N_4$ to produce single-layer g-$C_3N_4$ nanosheets.[34] The concentration of the g-$C_3N_4$ nanosheets can be tuned (0.1–3 mg mL$^{-1}$) by simply changing the volume ratio of the solvents. More importantly, the exfoliated nanosheets are stabilized against aggregation for more than six months.[34] The as-prepared g-$C_3N_4$ nanosheets exhibit superior photocatalytic activities toward the selective oxidation of benzyl alcohol and the degradation of rhodamine B with visible light compared to the layered counterparts.

Liquid ammonia assisted lithiation is also utilized as a simple, highly efficient, and rapid method to exfoliate bulky g-$C_3N_4$ into g-$C_3N_4$ nanosheets. Yin et al. showed that high-quality few-layer-thick g-$C_3N_4$ nanosheets were fabricated by liquid ammonia assisted lithiation.[38] Li intercalation was complete in less than 0.5 h, and importantly, the degree of Li intercalation was revealed by a change in the color of the liquid ammonia solution from deep blue to colorless. The lack of a high temperature or high-energy treatment resulted in a high-yield, and few-layer-thick g-$C_3N_4$ nanosheets with trace impurities of $O_2$ were produced. Interestingly, the surface structure as well as electronic and optical properties of the g-$C_3N_4$ nanosheets were significantly different from those of the parent bulk system, while the crystal structure and chemical stoichiometric ratio were similar. Moreover, compared to the bulk counterparts, the g-$C_3N_4$ nanosheets show clearly improved photocatalytic redox activity with respect to both $H_2$ evolution and generation of hydroxyl radicals.

The thermal exfoliation method appears to be a fast, low-cost, high-yielding, low-pollution, and environmentally friendly method for preparing g-$C_3N_4$ nanosheets. Niu et al. adopted a direct thermal oxidation etching process to attain g-$C_3N_4$ nanosheets (with a thickness of approximately 2 nm, corresponding to 6 to 7 layers) from bulk g-$C_3N_4$ (Figure 5b).[39a] The resultant nanosheets possess the features of a large surface area, small sheet thickness, increased bandgap, improved electron-transport ability along the in-plane direction, and prolonged lifetime of charge carriers as a result of the quantum confinement effect.[39] Importantly, the nanosheets exhibit higher photocatalytic activity toward $H_2$ evolution than the bulk g-$C_3N_4$ under irradiation with either UV/Vis and visible light.[39a] Xu et al. also used a thermal exfoliation method to prepare the graphene-analogous $C_3N_4$ materials from the g-$C_3N_4$-based intercalation compound (g-$C_3N_4$/$NH_4Cl$).[39b] These graphene-analogous g-$C_3N_4$ materials exhibited 2D thin-layer structures with a thickness of 2–3 nm (6–9 atomic layers), a high surface area (30 m$^2$ g$^{-1}$), increased photocurrent responses, and improved electron conductivity, which made it possible to achieve efficient photocatalytic activity in the degradation of methylene blue.[39b]

Thus, g-$C_3N_4$ nanosheets exhibit greatly improved photocatalytic activities compared with those of its bulk counterpart, likely because of the exceptionally high 2D anisotropy, the distinctive physicochemical properties and the unique electronic structures, such as large surface area, high reduction potential of the photogenerated electrons, increased photoelectric response, and fast charge-carrier separation.[34] Furthermore, the implication of the spherical nanostructures

of these 2D g-$C_3N_4$ nanosheets as scaffolds to assemble various functional motifs for artificial photosynthesis is of particular interest, as shown by the recent studies involving anchoring graphene oxide,[40] $TiO_2$,[41] CdS,[40,42] and ultrathin hexagonal $SnS_2$ nanosheets[43] onto g-$C_3N_4$ nanosheets. These 2D soft nanomaterials, made of one or several atomic layers, suggest appealing applications in the areas of electronics, catalysis, chemical and biological sensors, supercapacitors, gas separation, and energy storage.[44]

### 4.2. Template Approach

The template approach, which is based on the use of inorganic or organic nanostructures as templates, is one of the most effective methods to synthesize porous or nanoarchitectured materials.[45] The size, morphology, and pore structure can be simply modulated by the selection of different templates. Porous or nanoscale g-$C_3N_4$ materials can be manufactured by either the hard-template approach or soft-template approach.

#### 4.2.1. Hard-Template Approach

The hard-template method is a controllable, flexible, and precise strategy for the construction of a nanostructure. Hard templates are highly versatile and available for the design of different geometries that cover length scales from several nanometers over the micro- to the macroscale. This method also enables the construction of hierarchical pore architectures.

Mesoporous g-$C_3N_4$ materials are considered to be heterogeneous photocatalysts because of their large surface areas, accessible open pore walls, high light-harvesting ability, accelerated mass transfer, and unique semiconductor properties. The first mesoporous g-$C_3N_4$ (mpg-$C_3N_4$) photocatalyst was synthesized by the replication of silica nanoparticles with a size of 12 nm by using a thermal condensation process of cyanamide. mpg-$C_3N_4$ with different surface areas from 8 to 373 $m^2 g^{-1}$ can be obtained by altering the silica/cyanamide mass ratios from 0 to 1.5.[13b,46] Characterization results show that all mpg-$C_3N_4$ materials feature a mesoporous structure with a controlled surface area and a three-dimensionally interconnected framework with a semiconductor band gap of 2.7 eV. Importantly, the efficiency of $H_2$ evolution can be enhanced by approximately one order of magnitude by introducing mesoporosity into polymeric g-$C_3N_4$.[46]

The ordered mesostructure is important for enhancing the selectivity and activity in photocatalysis because it permits the structural orientation of guest molecules in the periodic nanopores and allows for easy assembly of catalytic cofactors into the structure. Ordered mesoporous g-$C_3N_4$ (ompg-$C_3N_4$) was synthesized by a nanocasting approach from a SBA-15 silica template.[46] The C/N ratio of the resulting material was 0.73:1, and semiconductive functions remained, as indicated by its yellow color, which is similar to bulk g-$C_3N_4$. Ompg-$C_3N_4$, which possesses a large surface area, uniform pore size, and a 2D accessible framework, exhibits improved activity for the photochemical reduction of water with visible light in the presence of Pt as a co-catalyst and electron trap.

In addition to the development of mesozeolitic g-$C_3N_4$, extensive efforts have been devoted to the synthesis of nanoshaped g-$C_3N_4$ from various templates. Numerous nanostructured g-$C_3N_4$ structures, including hollow g-$C_3N_4$ nanospheres (HCNS),[47] nanospherical g-$C_3N_4$ composed of nanosheets,[6a] helical g-$C_3N_4$ nanorods,[48] g-$C_3N_4$ nanosheets,[49] and diatom-shaped g-$C_3N_4$,[50] have been synthesized by using sacrificial templates, such as silica nanospheres, anodic aluminum oxide, chiral mesoporous silica, montmorillonite, and diatoms. For example, inspired by the structure of thylakoids in photosynthetic organisms in biological systems, the HCNSs, which were synthesized by using hollow silica nanospheres as templates, could serve as a light-harvesting platform for catalyzing $H_2$ evolution with visible light (Figure 6a).[47] Their inner optical reflection and scattering

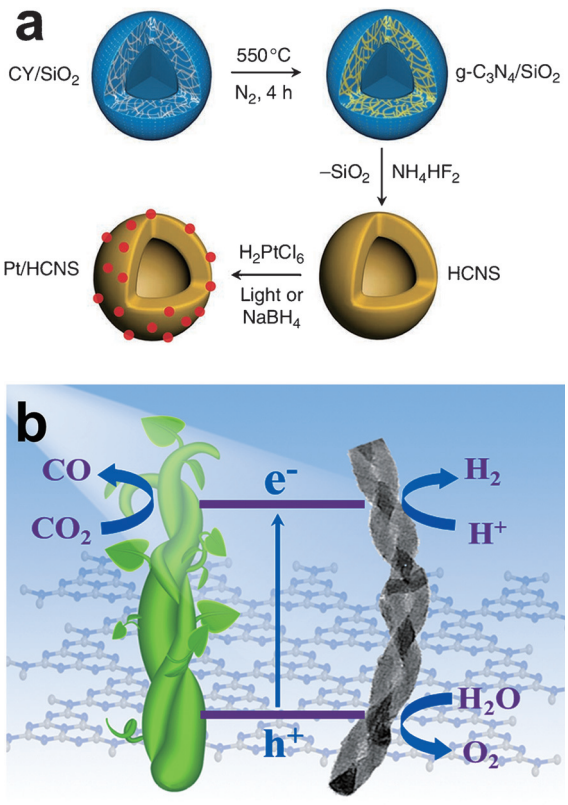


***Figure 6.*** a) Synthesis of HCNS and Pt/HCNS composites. Reprinted from Ref. [47]. Copyright 2012, Nature Publishing Group. b) Helical nanorod-like g-$C_3N_4$ for photocatalysis. Reproduced from Ref. [48b] with permission. Copyright 2014, Wiley-VCH.

provide a remarkably increased photochemical activity in hydrogen-evolution assays and achieve an apparent quantum yield of 7.5% at 420 nm. Moreover, the postannealing treatment is effective for reinforcing the interface/surface, improving the polymerization quality, and optimizing the texture of HCNS, which contributes to the surface reconstruction and superior photocatalytic activity for $H_2$ evolution.[51] This is a unique example of thermally and chemically

stable conjugated polymers with hollow nanostructures and optoelectronic properties. Such spherical hollow structures with enlarged interior and exterior surface areas can optimize both the capture and distribution of light and separate both the oxidative and reductive species in the nanoscale domain for the establishment of efficient light-induced redox catalysis in a cascading manner.[47,51] To further combine the advantages of nanospheres and nanosheets, a highly efficient photocatalyst—nanospherical g-$C_3N_4$ composed of nanosheets (NS-g-$C_3N_4$) with a highly open three-dimensional (3D) hierarchical framework assembled from 2D nanosheets with sharp edge tips—has been successfully fabricated by using spherical silica as the template.[6a] The open surface structures of the nanosheet with sharp edges can induce a similar promotion similar to a "lightning rod effect". This results in fast charge collection and separation at the tips, and a drastically improved $H_2$ evolution with a quantum yield of 9.6% at 420 nm is observed for 3 wt% Pt/NS-g-$C_3N_4$.[6a] Another typical example is helical g-$C_3N_4$ nanorods, which are fabricated using chiral mesoporous $SiO_2$ templates (Figure 6b).[48b] The helical nanoarchitectures promote the charge separation and mass transfer of g-$C_3N_4$ semiconductors, thereby enabling them to act as more-efficient photocatalysts for water splitting and $CO_2$ reduction than pristine g-$C_3N_4$.[48b] This is a novel example of chiral g-$C_3N_4$ that features both left- and right-handed helical nanostructures and exhibits unique optical activity to circularly polarized light at the semiconductor absorption edge.[48b] Thus, by choosing different templates with various nanostructures from 1D to 2D and 3D, g-$C_3N_4$ with various complex nanoarchitectures and morphologies can be obtained, and, in this manner, the properties and photocatalytic performances are also influenced.

The family of hard-template nanostructured g-$C_3N_4$ is extremely promising as a semiconductor scaffold for the construction of hybrid visible-light photocatalysts because it permits convenient functionalization by assembling chromophoric antenna molecules, water reduction co-catalysts, or water-oxidation complexes onto these host matrices, thus creating an innovative biomimetic photocatalyst system for water splitting chemistry but also for selective organic synthesis.[47,51] However, the use of hazardous fluoride-contained reagents to remove the template, multiple steps, and long experiment periods limit the applications of hard-templated synthesis.

#### 4.2.2. *Soft-Template Approach*

Compared with the hard-template approach, the "greener" soft-template route not only simplifies the entire synthetic procedure but also allows for easy tuning of the morphology through the choice of different soft templates. Soft structure-directing agents, such as surfactants, amphiphilic block polymers, or ionic liquids, can be utilized for the formation of nanostructured g-$C_3N_4$, thereby enabling the rational synthesis of materials with desired porous structures and surface morphologies by using different soft templates for specific uses.

Wang et al. prepared mesoporous g-$C_3N_4$ by the polycondensation of dicyandiamide with various soft templates, such as non-ionic surfactants, amphiphilic block polymers (e.g. Triton X-100, P123, F127, Brij30, Brij58, and Brij76) and some ionic surfactants (e.g. $BmimPF_6$, BmimDCN).[52] Most of the as-obtained products have a large surface area and high conductivity. However, two issues remained in this study. First, the formation of a useful pore system only exists in certain products from certain templates (e.g. Triton X-100 and ionic liquids). Second, the high carbon content of these materials interrupts the structure of g-$C_3N_4$ and lowers the photocatalytic performance.[52] To overcome these problems, Yan replaced dicyandiamide with melamine (a less-reactive precursor) and used Pluronic P123 as a template to synthesize mesoporous g-$C_3N_4$.[53] The as-obtained samples are wormlike porous g-$C_3N_4$ structures, featuring a small carbon content, a large surface area, a red-shifted absorbance edge, and photocatalytic reactivity for $H_2$ evolution (even at $\lambda > 700$ nm).[53]

In addition, ionic liquids have also been used as soft templates to react with dicyandiamide or urea to modify g-$C_3N_4$ nanoarchitectures (Figure 7).[52] The ionic liquid 1-butyl-3-methylimidazolium tetrafluoroborate can function as a multifunctional modifier for the self-polymerization of urea to control the texture, surface chemistry, and semiconductor properties of g-$C_3N_4$ in a simple one-pot manner.[52,54a] The obtained g-$C_3N_4$ nanosheets co-doped with B and F exhibit an improved photocatalytic performance for $H_2$ evolution compared with the pure g-$C_3N_4$.[52,54a] Following a similar strategy, P-doped g-$C_3N_4$ was prepared by using dicyandiamide and 1-butyl-3-methylimidazolium hexafluorophosphate. The resultant sample has a higher photocatalytic activity for decomposing rhodamine B and methyl orange than undoped g-$C_3N_4$.[16c] Considering the diversity of the ionic liquids family in terms of molecular structures and chemical compositions, the facile synthetic strategy using ionic liquids as soft

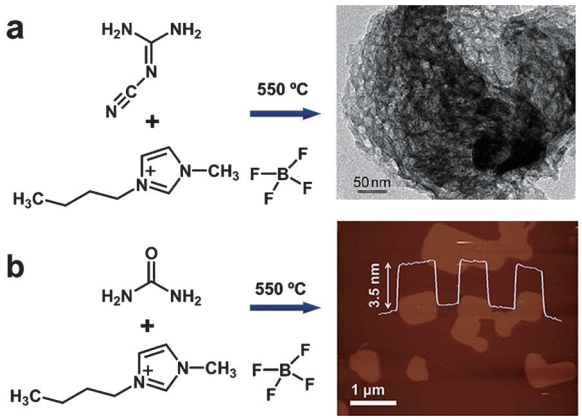


***Figure 7.*** B- and F-containing $C_3N_4$ synthesized by the polymerization of a) dicyandiamide and b) urea in the ionic liquid 1-butyl-3-methylimidazolium tetrafluoroborate. Reproduced from Ref. [52] with permission. Copyright 2010, Wiley-VCH, and Ref. [54a] with permission. Copyright 2014, Wiley-VCH.

modifiers for the preparation of heteroatom-containing g-$C_3N_4$ nanosheets can be regarded as an innovative method for tailoring the chemistry and morphology of conjugated g-$C_3N_4$ polymers for versatile applications.[54]

Nanostructured g-$C_3N_4$ can be synthesized using surfactants, amphiphilic block polymers, or ionic liquids as soft-templates by a self-polymerization reaction. The soft-template method opens up new avenues for the emerging applications of carbon nitride solids in the field of sustainable energy.

### 4.3. Supramolecular Preorganization Method

Compared to the above-mentioned template synthesis, the supramolecular preorganization method is a self-templating method that permits the synthesis of nanostructured materials without an external template or a post-treatment procedure for removing the template. The supramolecular approach is mainly based on the use of noncovalent interactions (e.g. hydrogen bonding) to form ordered building blocks for the desired synthesis.[55] Hydrogen bonds are significant for controlling molecular self-assembly because of their reversibility, specificity, and directionality.[55] The starting monomers will assemble into diverse structures in accordance with their ability to form hydrogen bonds in the solvent and create ordered and stable aggregates that consecutively define the final products.

Recently, the supramolecular preorganization of monomers or triazine molecules has emerged as an appealing approach to modify the morphology, texture, and photophysical properties of g-$C_3N_4$.[56] Nanostructured g-$C_3N_4$ photocatalysts can be synthesized by the supramolecular preorganization of hydrogen-bonded molecular assemblies, such as cyanuric acid/melamine,[57] melamine/cyanuric acid (MCA),[58] or melamine/trithiocyanuric acid[58] mixtures. For example, ordered hollow g-$C_3N_4$ structures, generated using a cyanuric acid/melamine complex in ethanol as a starting product, feature a significantly reduced fluorescence intensity and lifetime, accelerated charge transfer, and a dramatic enhancement in the photocatalytic activity for the degradation of rhodamine B.[57] Moreover, the morphologies of the cyanuric acid/melamine complex (and thus the ordered g-$C_3N_4$ architectures) can be altered by using different solvents.[57] Jun et al. prepared mesoporous hollow spheres comprised of tri-*s*-triazine-based g-$C_3N_4$ nanosheets by the thermal polycondensation of flowerlike, layered spherical supramolecular aggregates of a melamine/cyanuric acid complex under nitrogen at 550 °C.[58a] The layered structure generated from the melamine/cyanuric acid complex induces greater utilization of light, broadens the band gap by 0.16 eV, and prolongs the lifetime of photoexcited charge carriers twofold compared to the bulk g-$C_3N_4$.[58a] Thus, the photodegradation of rhodamine B on the catalyst can be accelerated tenfold, even without the aid of cofactors, such as $H_2O_2$ and metal ions.[58a] The same authors also developed 3D macroscopic assemblies of low-dimensional g-$C_3N_4$ (such as nanoparticles, nanotubes, and nanosheets) as efficient catalysts for the photocatalytic evolution of $H_2$.[58b] By controlling the ratio of monomers, precipitation temperature, solvent, and hydrogen-bonding donor–acceptor pairs, the structure, morphologies, as well as absorption and emission properties of the hydrogen-bonded molecular assembly of triazine molecules (and thus the resulting g-$C_3N_4$) can be rationally modulated (Figure 8).[58b]

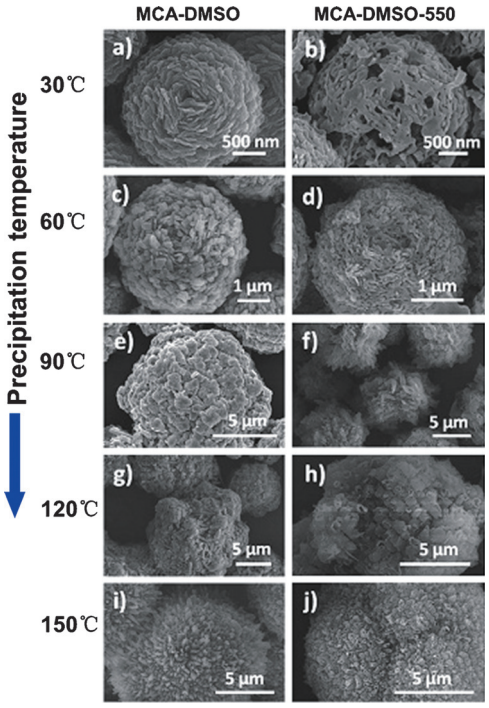


***Figure 8.*** SEM images of as-synthesized MCA-DMSO (left) and the corresponding MCA-DMSO-550 (right) precipitated at a,b) 30, c,d) 60, e,f) 90, g,h) 120, and i,j) 150 °C. The melamine/cyanuric acid is denoted as MCA. Reproduced from Ref. [58b] with permission. Copyright 2013, Wiley-VCH.

Moreover, both the tailoring of the morphology and design of the chemical structure of g-$C_3N_4$ can be realized by integration of the supramolecular approach with a molecular design strategy.[56] For example, Ishida et al. modified a g-$C_3N_4$ photocatalyst by adopting triple supramolecular complexes of cyanuric acid, melamine, and 2,4-diamino-6-phenyl-1,3,5-triazine as precursors. The as-obtained g-$C_3N_4$ photocatalyst exhibits a large surface area and defined morphology, improved light absorption in the visible region, as well as superior activity in the photodegradation of rhodamine B, up to 16-fold higher than that of bulk g-$C_3N_4$.[56] Changes in the ratio of the three raw monomers resulted in different morphologies, absorption, and emission properties, along with the incorporation of different numbers of phenyl groups in the resulting g-$C_3N_4$ structures. Following a similar strategy, an efficient roll-like g-$C_3N_4$ photocatalyst has been prepared by using a supramolecular complex composed of cyanuric acid, melamine, and barbituric acid as the starting monomers.[55] The self-organization and copolymerization with barbituric acid results in a red-shift of the absorption edge into the visible region as well as the in situ formation of in-plane heterojunctions that accelerate the charge separation

process.[55] Additionally, upconversion agents have also been used to modify g-$C_3N_4$ by the direct thermal condensation of a mixture of $ErCl_3{\cdot}6H_2O$ and the supramolecular precursor cyanuric acid/melamine.[55] Doping with $Er^{3+}$ modulated both the electronic and chemical properties of g-$C_3N_4$ and increased the photocatalytic activity of g-$C_3N_4$ for the decomposition of rhodamine B dye with visible light.[55]

Therefore, the supramolecular approach constitutes a self-templating synthetic pathway for the facile one-pot preparation of efficient g-$C_3N_4$ photocatalysts and opens up new vistas for the optimization of structure, texture, and optical properties of g-$C_3N_4$ for the creation of efficient photoactive materials.[57] However, the choice of precursors is limited because not all precursors will form hydrogen bonds in a solvent. The assembly process is greatly affected by many external factors, and the stability of the hydrogen-bonded molecular assemblies should not be ignored.

### 4.4. Solvothermal Technology

Solvothermal synthesis occurs under sub-/supercritical conditions in a closed system in the presence of an aqueous/non-aqueous solvent at a temperature higher than the boiling temperature of the solvent. This soft solution-processing approach allows for the bottom-up design of material structure in a one-pot manner by molecular design, solution assembly, crystallization, and covalent cross-linking chemistry.[59] In addition, solvothermal techniques enable the assembly of large polymeric superstructures at relatively low temperature.[59] Low-temperature conditions for synthesis are beneficial for g-$C_3N_4$ materials because the electronic and chemical structures of g-$C_3N_4$ can be easily modified by abundant organic chemistry procedures, and nitrogen depletion from g-$C_3N_4$ solids can be effectively prevented at moderate temperatures.[59]

Montigaud et al. synthesized g-$C_3N_4$ through the condensation of melamine and cyanuric chloride by using isopropylethylamine as the solvent and base catalyst at 250 °C and 130 MPa.[60] Our group demonstrated that g-$C_3N_4$ superstructures involving nanorod networks were fabricated by solvothermal synthesis through the polycondensation of cyanuric chloride and melamine in hot acetonitrile at 180 °C for 96 h (Figure 9).[59] The resultant g-$C_3N_4$ exhibits a diminished band gap, improved light-harvesting properties, and photocatalytic reactivity for pollutant degradation and water splitting.[59] Although the ability of the g-$C_3N_4$ to generate $H_2$ was merely comparable to that of conventional g-$C_3N_4$, and the resultant sample from the solvothermal synthesis features low crystallinity, the relatively low temperature without the addition of catalysts is a breakthrough in g-$C_3N_4$ synthesis.[59] Moreover, this solvothermal route can be integrated with numerous modification approaches to establish new pathways for the design of highly efficient g-$C_3N_4$-based semiconductors in solution. Thus, the chemical composition, electronic structure, and surface functionality of g-$C_3N_4$ will be better engineered for broader applications in catalysis, energy conversion, and environmental remediation.[59]

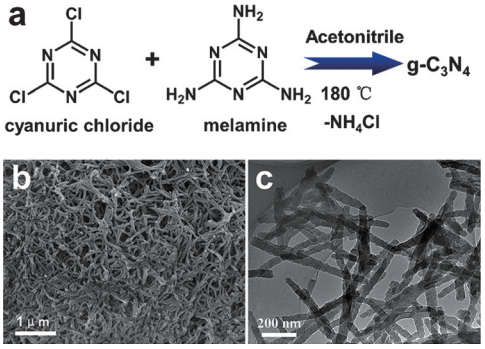


*Figure 9.* a) Solvothermal synthetic processes of g-$C_3N_4$ from cyanuric chloride and melamine in acetonitrile as the solvent at 180 °C. b) SEM images and c) TEM images of the as-synthesized g-$C_3N_4$. Reproduced from Ref. [59] with permission. Copyright 2012, Wiley-VCH.

### 4.5. Other Methods

Aside from the above methods, other methods have also been utilized for the synthesis of nanostructured g-$C_3N_4$. The choice of different precursors significantly influences the texture and morphology of the resultant g-$C_3N_4$ samples. For example, directly heating melamine hydrochloride could result in more pores in the final g-$C_3N_4$ with a large surface area (39-fold greater), accompanied by an increase in the band gap of 0.13 eV.[61] The increased porosity significantly enhanced the photoreactivity of g-$C_3N_4$ for the photooxidation of rhodamine B by 9.4-fold, but lowered its activity in the photoreduction of $CO_2$ 4.6-fold.[61]

By rationally controlling the polymerization process of melamine, distorted g-$C_3N_4$ nanosheets were synthesized without relying on any additional species (Figure 10a).[62]

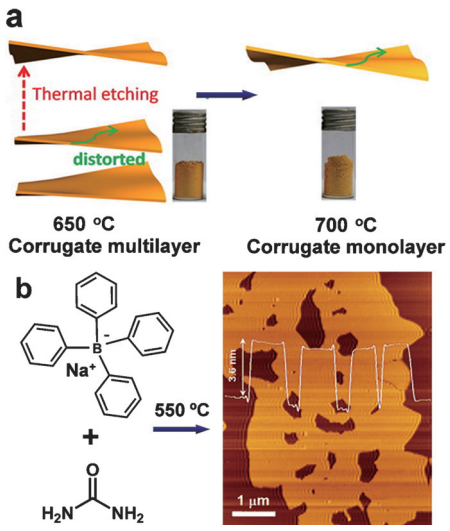


*Figure 10.* a) Fabrication of structurally distorted $C_3N_4$ nanosheets. Reproduced from Ref. [62] with permission. Copyright 2014, American Chemical Society. b) Synthesis and atomic force microscopy (AFM) images of B-modified $C_3N_4$ nanosheets. The white line shows the height profile of B-modified $C_3N_4$ nanosheets from the AFM image. Reproduced from Ref. [63] with permission. Copyright 2013, Wiley-VCH.

The distorted g-$C_3N_4$ exhibited structure-distortion-induced extension in the optical absorption by activation of the $n\rightarrow\pi^*$ transitions in the aromatic system and improved the photocatalytic activity for water splitting. Its wavelength-dependence activity can be extended to 550 nm with good production of hydrogen.[62] Experimental results and theoretical calculations both demonstrated that the band structure is affected by the structural distortion and number of layers, whereas in-plane basic units remain intact and the connecting modes remain invariable during the peeling process.[62]

Co-condensation of urea and sodium tetraphenylboron afforded B-modified g-$C_3N_4$ nanosheets that were applied as the photocatalyst for the hydrogen evolution reaction.[63] These g-$C_3N_4$ nanosheets with reduced layer thicknesses and strengthened surface reactivity can be regarded as promising 2D light-harvesting transducers for the sustainable harnessing of solar energy for hydrogen photosynthesis (Figure 10b).[63]

## 5. Crystal-Structure Engineering

Synthesis in molten salts opens up great opportunities for the synthesis of crystalline, condensed g-$C_3N_4$,[7] which is also a kind of covalent organic/polymeric framework. The well-known problem of the insufficient crystallinity of the carbon nitride condensation products could be overcome by using the ionothermal approach.[64] More recently, the triazine-based g-$C_3N_4$, which was predicted in 1996, has been successfully prepared by using the ionothermal reaction for the first time, and is different from melon-based g-$C_3N_4$ materials.[65]

The 2D layered network of g-$C_3N_4$ can be obtained as an intercalation compound with halides from the ionothermal condensation of dicyandiamide/melamine in a eutectic salt melt (e.g. KCl/LiCl, KBr/LiBr, and LiCl·$H_2O$/KCl/NaCl).[7b,65,66] Bojdys et al. reported the synthesis of a crystalline g-$C_3N_4$ based on sheets of hexagonally arranged *s*-heptazine ($C_6N_7$) units by the temperature-induced condensation of dicyandiamide by using a salt melt of lithium chloride and potassium chloride as the solvent.[7a] Detailed structural characterization proved that the as-prepared product (*P*6-*cm*, no. 185; $a = 846.82$, $c = 675.02$ pm) is a 2D network composed of essentially planar layers comprised of nitrogen-bridged heptazine units, different from Liebig's melon formed by the traditional bulk condensation route.[7a] Voids in these layers are stacked upon each other, thereby forming channels running parallel to [001] that are filled with $Li^+$ and $Cl^-$ ions.[7b] Wirnhier et al. adopted a LiCl/KCl salt melt to prepare a 2D poly(triazine imide) (PTI) with high crystallinity.[7b] The NMR data ruled out the presence of heptazine units in PTI/$Li^+Cl^-$ and corroborate a triazine-based structure model.[7b] Ham et al. suggested that the presence of LiCl during the synthesis plays a crucial role in stabilizing the *s*-triazine unit in conditions under which the more stable tri-*s*-triazine unit would otherwise form.[64a] The band gap of the PTI/$Li^+Cl^-$ material is tunable through controlling the LiCl loading, with a minimum gap of 2.2 eV when fully loaded.[67]

As PTI/$Li^+Cl^-$ has a graphitic structure, the new type of carbon nitride also possess a band structure suitable for the photocatalytic splitting of water.[64a] Ham et al. showed that PTI/$Li^+Cl^-$, modified with either Pt or $CoO_x$ as a co-catalyst, photocatalytically produced $H_2$ or $O_2$, respectively.[64a] The production of $H_2$ or $O_2$ from water indicates that the valence and conduction bands of PTI/$Li^+Cl^-$ were properly located to achieve overall water splitting.[64a] Zou and co-workers reported that a carbon nitride intercalation compound synthesized by a simple molten salt route is an efficient polymer photocatalyst for solar hydrogen production with visible-light irradiation.[64b] The effect of alkali coordination on the photocatalytic reactivity has been analyzed.[64b] Coordinating the alkali metals into the C-N plane of carbon nitride will induce a non-uniform spatial charge distribution; although the electrons are confined in the intercalated region, the holes are in the far intercalated region, which promotes efficient separation of photogenerated carriers.[64b] The coordination of donor-type alkali metal atoms into the nitrogen positions of carbon nitrides increases the concentration of free carriers and leads to the formation of novel nonradiative paths.[64b] Thus, the coordination of alkali metal atoms should favor improved transport of the photogenerated electron and hole and decrease the electron–hole recombination rate.[64b]

Recently, Algara-Siller et al. succeeded in constructing macroscopically large, crystalline thin films of triazine-based g-$C_3N_4$ by using dicyandiamide. The films consist of stacked 2D crystals with thicknesses between a few and several hundreds of atomic layers.[65] Characterization shows a long-range, in-plane ordered structure.[65] Experimental and computational data support a corrugated layer structure and a direct bandgap between 1.6 and 2.0 eV, which provides new possibilities for new building blocks for electronic devices.[65]

Crystalline 2D carbon nitride can be exfoliated into nanosheets by mechanical and chemical routes. Bojdys et al. reported that bromide-intercalated PTI can be exfoliated by intercalation of K and subjecting the intercalate to water.[68] The resulting thin sheets show large lateral sizes in the micrometer range; however, such ranges are expected to be unfavorable for photocatalysis due to the relatively small surface area and exposed number of defective sites.[68] Schwinghammer et al. demonstrated the one-step synthesis of crystalline PTI nanosheets by liquid-phase exfoliation in water without the need for additives, toxic solvents, or preintercalation steps (Figure 11).[69] Remarkably, facile exfoliation in water leads to highly crystalline nanosheets of 1–2 nm in thickness with chemical and colloidal stability, which show significantly increased photocatalytic efficiency for visible-light-driven hydrogen evolution compared to bulk crystalline PTI.[69] This study highlights the crucial role of morphology and surface area in the photocatalytic performance of g-$C_3N_4$ materials.[69]

Controlling the amount and arrangement of dopants during the polycondensation of g-$C_3N_4$ in an ionic melt dramatically enhances the photoactivity for $H_2$ evolution. Lotsch and co-workers synthesized 2D triazine-based $C_3N_4$ in a two-step ionothermal synthesis by using 4-amino-2,6-dihydroxypyrimidine as the dopant.[70] A rather low level of structural definition and the introduction of defects up to a certain doping level (16% for 4-amino-2,6-dihydroxypyr-

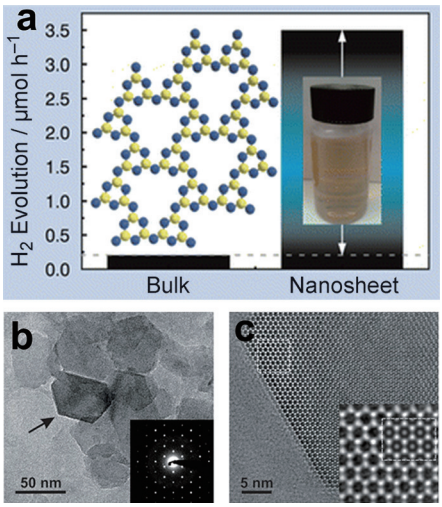


***Figure 11.*** a) Photocatalytic activity of $H_2$ production of the Pt/PTI nanosheets and Pt/bulk-PTI. The inset shows an idealized PTI structure (lithium/chloride intercalation omitted for clarity) and a photograph of a liquid PTI nanosheet suspension. b) TEM image of the exfoliated ultrathin PTI nanosheets. c) Higher-magnification TEM image of a PTI nanosheet edge viewed along [001] and simulation (JEMS; $\Delta f = +50$ nm, $t = 2.70$ nm; inset). Reproduced from Ref. [69] with permission. Copyright 2014, American Chemical Society.

imidine) tend to enhance the photoactivity.[70] This 2D triazine-based g-$C_3N_4$ shows substantial visible-light-induced $H_2$ production from water, with external quantum efficiencies as high as 3.4%, which rivals the benchmark of heptazine-derived photocatalysts.[70] However, although Lotsch and co-workers utilized an ionothermal synthetic method, their g-$C_3N_4$ materials are typically amorphous.[70] Thus, it is essential to develop new strategies for the rational preparation of g-$C_3N_4$ photocatalysts to further enhance their crystallinity and photocatalytic efficiencies.

Bhunia et al. obtained the triazine-based crystalline g-$C_3N_4$ through the combination of supramolecular aggregation and polycondensation in an ionic melt by using melamine as a precursor and 2,4,6-triaminopyrimidine as a dopant.[71] The improved condensation provides high crystallinity and a remarkably increased photoactivity for $H_2$ evolution, with a quantum yield of about 7% at 420 nm.[71] The two-step rearrangement process, supramolecular aggregation, and polycondensation in the ionic melt, together with controlled modification of the chemically compatible dopant is a promising route for the rational design of photoactive crystalline g-$C_3N_4$ from a diverse range of inexpensive precursors.[71]

Thus, g-$C_3N_4$ materials can be obtained as an intercalation compound with halides and nanosheets from ionothermal condensation in a eutectic salt melt. The poly(triazine imide) synthesized from the ionothermal approach shows improved structure, higher crystallinity, and an increased photoactivity. Coupling the polycondensation process in an ionic melt with nanostructure engineering, copolymerization, and supramolecular assembly provides a feasible pathway for the synthesis of highly effective g-$C_3N_4$. The widespread availability of organic/inorganic dopants permits the rational design of a broad range of triazine-based g-$C_3N_4$ structures with modified functions.[70] The easily adjustable crystallinity as well as structural and electronic properties of g-$C_3N_4$ renders them particularly versatile for the conversion of solar energy.[70]

## 6. Heterostructure Construction

The formation of heterostructures has become a common and feasible strategy to accelerate the electron–hole separation and improve the photocatalytic efficiency of g-$C_3N_4$.[72] The heterostructured composite photocatalysts based on g-$C_3N_4$ materials are composed of wide bandgap inorganic semiconductor/g-$C_3N_4$, narrow bandgap inorganic semiconductor/g-$C_3N_4$, carbon/g-$C_3N_4$, polymer/g-$C_3N_4$, and g-$C_3N_4$-based ternary heterostructures.

Firstly, we consider wide bandgap inorganic semiconductor/g-$C_3N_4$ composite catalysts. For example, a core/shell structured g-$C_3N_4$/$BiPO_4$ photocatalyst exhibits a higher photocatalytic activity under UV irradiation than P25 ($TiO_2$) and $BiPO_4$.[72] A concept for the separation and transport of photogenerated electron–hole pairs at the g-$C_3N_4$/$BiPO_4$ interface has been proposed.[72] $BiPO_4$ can be excited by UV light to generate photoinduced electron–hole pairs; then, the photogenerated holes on $BiPO_4$ can migrate to g-$C_3N_4$ because the position of the valence band of $BiPO_4$ is lower than the HOMO of g-$C_3N_4$. Thus, charge separation is facilitated, thereby lowering the recombination rate of photogenerated electron–hole pairs and resulting in an enhancement in the photocatalytic activity.[72]

Second, we consider narrow bandgap inorganic semiconductor/g-$C_3N_4$ composites. For example, the activity of the composite photocatalyst g-$C_3N_4$/TaON for the photodegradation of rhodamine B is higher than that of either single-phase g-$C_3N_4$ or TaON.[73] A scheme for electron–hole separation and transport at the g-$C_3N_4$/TaON composites has been proposed.[73] The electrons on the g-$C_3N_4$ surfaces can transfer smoothly to TaON via the well-defined interface because the conduction band edge potential of g-$C_3N_4$ (−1.12 eV) is lower than that of TaON (−0.34 eV), whereas the photogenerated holes on the TaON surface can easily migrate to g-$C_3N_4$ because of the large difference in the potentials of the valance band edges.[73] The electron–hole separations are also driven by the internal rebuilt electric fields in the two semiconductors.[73] This process contributes to a large number of electrons on the TaON surface and more holes on the g-$C_3N_4$ surface, which lowers the probability of electron–hole recombination and promotes the photocatalytic activity.[73] In addition, $MoS_2$/g-$C_3N_4$ heterojunctions were synthesized by impregnating g-$C_3N_4$ with an aqueous solution of $(NH_4)_2MoS_4$, and subsequent sulfidation with $H_2S$ gas at 350°C (Figure 12a).[74a] These $MoS_2$/g-$C_3N_4$ layered junctions exhibit significantly enhanced photocatalytic activities of $H_2$ evolution because of the large contact area and efficient absorption of light, along with rapid charge separation.[74a] This study not only symbolizes a proof of concept for the construction of thin interfacial junctions between semiconductors and co-catalysts featuring analogous layered geometric structures, but also shows the possibility for the

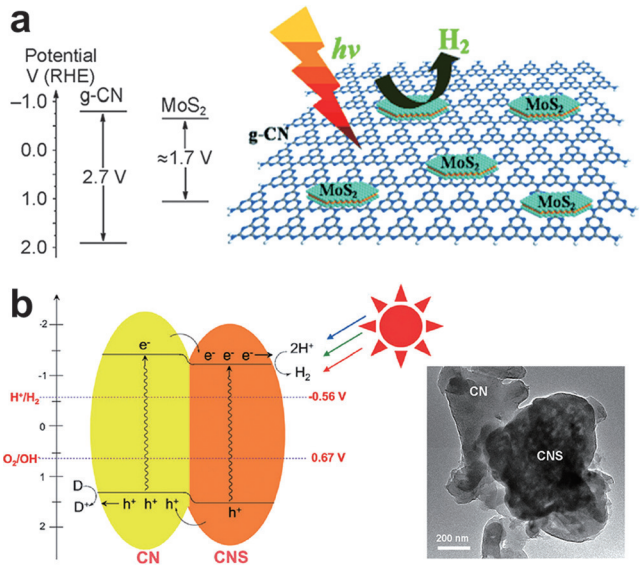


***Figure 12.*** a) Idealized structural model of the $MoS_2$/g-$C_3N_4$ layered junctions for hydrogen evolution, and band energy diagrams for g-$C_3N_4$ and thin $MoS_2$. Reproduced from Ref. [74a] with permission. Copyright 2013, Wiley-VCH. b) Organic heterojunction CN/CNS formed between carbon nitride (CN) and sulfur-mediated carbon nitride (CNS), and typical TEM images of CN/CNS (D = donor). Reproduced from Ref. [76a] with permission. Copyright 2012, Wiley-VCH.

utilization of low-cost noble-metal-free catalysts for efficient photocatalytic evolution of $H_2$ with visible light.[74]

Third, we consider carbon/g-$C_3N_4$ composites. Yu and co-workers reported the photocatalytic activity of graphene/g-$C_3N_4$ composites toward $H_2$ production.[75] The incorporation of graphene sheets as electron-conducting channels can facilitate electron transfer and enhance the photocatalytic activity.[75] Since then, many carbon materials, such as graphene, graphene oxide, reduced graphene oxide, carbon nanotubes, $C_{60}$, and ordered mesoporous carbon, have been coupled with g-$C_3N_4$ as efficient metal-free composite photocatalysts.

Fourth, we consider the polymer/g-$C_3N_4$ heterostructure. Isotype heterojunctions of carbon nitride/sulfur-mediated carbon nitride (CN/CNS) were constructed according to the alignment of bands between the two types of g-$C_3N_4$ and the slight difference in their electronic band structures (Figure 12b).[76a] Such a polymeric isotype heterojunction promotes charge separation as a consequence of the band offsets and significantly enhances the photocatalytic activity for $H_2$ evolution.[76a] The heterostructure strategy provides new insights into constructing an isotype/anisotype dyadic layering on the various nanostructured and copolymerized g-$C_3N_4$ frameworks to improve exciton dissociation and charge separation.[76a] Binary composites of polyaniline nanorods grown on the surface of g-$C_3N_4$ sheets were used as the photocatalyst for degrading methylene blue and methyl orange.[76b] The synergistic effect of g-$C_3N_4$ and polyaniline results in effective charge separation, a large surface area, and an increased photocatalytic activity.[76b] The superior photocatalytic activity and high stability of polymer-g-$C_3N_4$ composites render them promising photocatalysts for water splitting and pollutant degradation.[76b]

Finally, ternary composites composed of g-$C_3N_4$ have been constructed for photocatalytic reactions. A ternary composite of graphene, g-$C_3N_4$, and poly(3-hexylthiophene) ($P_3HT$) was used as an efficient photocatalyst for the degradation of pollutants.[77a] The degradation rate of methylene blue on a graphene-g-$C_3N_4$-$P_3HT$ ternary polymer composite is three-fold higher than that achieved by a g-$C_3N_4$-$P_3HT$ composite.[77a] The efficient charge transfer between graphene and g-$C_3N_4$-$P_3HT$ is seemingly responsible for the enhanced photocatalytic activity.[77a]

These studies, together with the emerging modification of g-$C_3N_4$ with enzymes, bio-inspired species, and cobalt co-catalysts[77b–d] offer new inroads into the exploration and utilization of heterostructure and heterojunction materials for environmental and photochemical applications.

## 7. Applications of g-$C_3N_4$ in Photoredox Catalysis

A variety of g-$C_3N_4$-based photocatalysts have been utilized in versatile redox reactions, including water splitting, $CO_2$ conversion, pollutant decomposition, bacterial inactivation, organic synthesis, and photoelectronic device.[78–90]

Tang and co-workers have constructed two parallel systems for overall water splitting (both $H_2$ and $O_2$ can be evolved in an ideal ratio of 2:1) with visible light by using g-$C_3N_4$ with two different metal oxides, $BiVO_4$ and $WO_3$.[79] A photosystem for the conversion of $CO_2$ into CO was designed by using g-$C_3N_4$ as both the $CO_2$ activator and photocatalyst, and the cobalt bipyridine complex ($[Co(bpy)_3]^{2+}$) as a redox promoter. A quantum yield of 0.25% at 420 nm was obtained,[80b] whilst Maeda and co-workers grafted ruthenium complexes onto the surface of g-$C_3N_4$ photocatalysts to convert $CO_2$ into formic acid with a quantum yield of 2%.[80c,d] Yu et al. showed that g-$C_3N_4$ photocatalysts can decompose organic pollutants such as rhodamine B, methylene blue, and formaldehyde.[81c] Huang et al. reported that g-$C_3N_4$ materials exhibit bacterial inactivation effects on *E. coli* K-12 in water under irradiation with visible light.[82] In addition, g-$C_3N_4$-based materials have also been shown to act as multifunctional photocatalysts for organic redox synthesis in general, such as the selective oxidation of organic compounds (e.g. amines, alcohols, and benzene), as well as the photocatalytic regeneration of $NAD^+$ to NADH to establish tandem catalysis.[83–86] These studies demonstrate the great potential of polymeric g-$C_3N_4$ materials for a broad range of solar applications based on photoredox catalysis.

## 8. Conclusions and Perspectives

Recent years have witnessed a fast growing interest in designing polymeric g-$C_3N_4$ photocatalysts. As a metal-free polymeric photocatalyst with a band gap of 2.7 eV, pristine g-$C_3N_4$ suffers from some shortcomings compared to inorganic photocatalysts, including high exciton binding energy, small surface area, limited light-harvesting capability, and fast

  

recombination of charge. In addition, the poor crystallinity and many surface defects in polymeric g-$C_3N_4$ restrict its photocatalytic applications.

The development of diverse synthetic techniques and physicochemical strategies to endow g-$C_3N_4$ solids with an optimized electronic structure, nanostructure, crystal structure, and heterostructure has become an urgent necessity to increase the photocatalytic performance of g-$C_3N_4$. First, doping is as an effective procedure to adjust the redox potentials of charge carriers and enhance the optical absorption by introducing foreign impurities into g-$C_3N_4$, whereas copolymerization is desirable to extend the delocalization of the $\pi$ electrons and change the intrinsic semiconductor properties by grafting aromatic groups onto the surface of the g-$C_3N_4$. These two methods enable the modulation of the molecular structure, electronic structure, and photocatalytic activity of g-$C_3N_4$. Second, numerous nanostructured g-$C_3N_4$ materials have been prepared by various synthetic pathways, including the exfoliation strategy, the hard/soft templating strategy, solvothermal technology, the supramolecular preorganization approach, and other methods. In general, nanoarchitectured g-$C_3N_4$ tends to show an outstanding photocatalytic performance compared to the bulk counterpart, probably because of the favorable surface properties, optimized electronic structure, accelerated charge separation, as well as promoted mass diffusion during photoredox reactions. Third, modulating the crystal structure of g-$C_3N_4$ by polycondensation in an ionic melt remarkably enhances the photocatalytic activity of g-$C_3N_4$. Finally, creating heterostructure photocatalysts by combining g-$C_3N_4$ and other semiconductors with energetically matching band structures is an effective method to realize fast separation of photoinduced charge carriers and high photocatalytic activities. Thus, with the reasonable design of the structure of g-$C_3N_4$ at different scales, the photocatalytic applications of g-$C_3N_4$ would be significantly enriched in a more rational manner.

Although significant effort has already been devoted to the modificataion of g-$C_3N_4$ materials and optimizing their photocatalytic activity, the potential of g-$C_3N_4$ materials has yet to be exploited fully. The main challenges that must be overcome for g-$C_3N_4$ involve 1) the synthesis of 600 nm class g-$C_3N_4$ photocatalysts with bandgaps of 1.8–2.0 eV (corresponding to optical absorption of ca. 600–700 nm)[91] and with high electric conductivity, and 2) the control of surface kinetics on g-$C_3N_4$, namely, how to promote charge separation and selective migration on g-$C_3N_4$ by taking account of both the design of the surface junction and texture engineering. Texture engineering brings the idea of creating membrane and core–shell structures for the controlled deposition of oxidation and reduction cofactors for the control of electron and hole transfer at the interface for overall water splitting. There will be extensive opportunities related to the utilization of g-$C_3N_4$ in sustainable catalysis, solar energy conversion, and devices, which will require much effort from researchers and scientists worldwide.

*This work is supported by the National Basic Research Program of China (2013CB632405), the National Natural Science Foundation of China (21425309 and 21173043), and the Specialized Research Fund for the Doctoral Program of Higher Education (20133514110003).*

**How to cite:** *Angew. Chem. Int. Ed.* **2015**, *54*, 12868–12884
*Angew. Chem.* **2015**, *127*, 13060–13077

[1] A. Fujishima, K. Honda, *Nature* **1972**, *238*, 37–38.
[2] a) Y. Zheng, Z. M. Pan, X. C. Wang, *Chin. J. Catal.* **2013**, *34*, 524–535; b) S. J. Liang, L. R. Wen, S. Lin, J. H. Bi, P. Y. Feng, X. Z. Fu, L. Wu, *Angew. Chem. Int. Ed.* **2014**, *53*, 2951–2955; *Angew. Chem.* **2014**, *126*, 2995–2999; c) K. Maeda, T. Takata, M. Hara, N. Saito, Y. Inoue, H. Kobayashi, K. Domen, *J. Am. Chem. Soc.* **2005**, *127*, 8286–8287.
[3] a) X. C. Wang, K. Maeda, A. Thomas, K. Takanabe, G. Xin, J. M. Carlsson, K. Domen, M. Antonietti, *Nat. Mater.* **2009**, *8*, 76–80; b) J. S. Zhang, J. H. Sun, K. Maeda, K. Domen, P. Liu, M. Antonietti, X. Z. Fu, X. C. Wang, *Energy Environ. Sci.* **2011**, *4*, 675–678; c) F. J. Zhang, F. Z. Xie, S. F. Zhu, J. Liu, J. Zhang, S. F. Mei, W. Zhao, *Chem. Eng. J.* **2013**, *228*, 435–441.
[4] X. C. Wang, S. Blechert, M. Antonietti, *ACS Catal.* **2012**, *2*, 1596–1606.
[5] Y. F. Sun, S. Gao, F. C. Lei, C. Xiao, Y. Xie, *Acc. Chem. Res.* **2015**, *48*, 3–12.
[6] a) J. S. Zhang, M. W. Zhang, C. Yang, X. C. Wang, *Adv. Mater.* **2014**, *26*, 4121–4126; b) J. S. Zhang, F. S. Guo, X. C. Wang, *Adv. Funct. Mater.* **2013**, *23*, 3008–3014.
[7] a) M. J. Bojdys, J. O. Müller, M. Antonietti, A. Thomas, *Chem. Eur. J.* **2008**, *14*, 8177–8182; b) E. Wirnhier, M. Döblinger, D. Gunzelmann, J. Senker, B. V. Lotsch, W. Schnick, *Chem. Eur. J.* **2011**, *17*, 3213–3221.
[8] M. Xu, L. Han, S. J. Dong, *ACS Appl. Mater. Interfaces* **2013**, *5*, 12533–12540.
[9] a) A. Thomas, A. Fischer, F. Goettmann, M. Antonietti, J. O. Muller, R. Schlogl, J. M. Carlsson, *J. Mater. Chem.* **2008**, *18*, 4893–4908; b) Y. J. Zhang, T. Mori, J. H. Ye, *Sci. Adv. Mater.* **2012**, *4*, 282–291; c) Y. Zheng, J. Liu, J. Liang, M. Jaroniec, S. Z. Qiao, *Energy Environ. Sci.* **2012**, *5*, 6717–6731; d) Y. Wang, X. C. Wang, M. Antonietti, *Angew. Chem. Int. Ed.* **2012**, *51*, 68–89; *Angew. Chem.* **2012**, *124*, 70–92; e) J. J. Zhu, P. Xiao, H. L. Li, S. A. C. Carabineiro, *ACS Appl. Mater. Interfaces* **2014**, *6*, 16449–16465; f) G. P. Dong, Y. H. Zhang, Q. W. Pan, J. R. Qiu, *J. Photochem. Photobiol. C* **2014**, *20*, 33–50.
[10] J. V. Liebig, *Ann. Pharm.* **1834**, *10*, 10.
[11] a) D. M. Teter, R. J. Hemley, *Science* **1996**, *271*, 53–55; b) K. Maeda, X. C. Wang, Y. Nishihara, D. L. Lu, M. Antonietti, K. Domen, *J. Phys. Chem. C* **2009**, *113*, 4940–4947; c) Y. Xu, S. P. Gao, *Int. J. Hydrogen Energy* **2012**, *37*, 11072–11080.
[12] Y. J. Cui, Z. X. Ding, P. Liu, M. Antonietti, X. Z. Fu, X. C. Wang, *Phys. Chem. Chem. Phys.* **2012**, *14*, 1455–1462.
[13] a) B. Jürgens, E. Irran, J. Schneider, W. Schnick, *Inorg. Chem.* **2000**, *39*, 665–670; b) M. Groenewolt, M. Antonietti, *Adv. Mater.* **2005**, *17*, 1789–1792.
[14] H. Tong, S. X. Ouyang, Y. P. Bi, N. Umezawa, M. Oshikiri, J. H. Ye, *Adv. Mater.* **2012**, *24*, 229–251.
[15] a) M. Pfeiffer, K. Leo, X. Zhou, J. S. Huang, M. Hofmann, A. Werner, J. Blochwitz-Nimoth, *Org. Electron.* **2003**, *4*, 89–103; b) S. C. Erwin, L. J. Zu, M. I. Haftel, A. L. Efros, T. A. Kennedy, D. J. Norris, *Nature* **2005**, *436*, 91–94.
[16] a) S. C. Yan, Z. S. Li, Z. G. Zou, *Langmuir* **2010**, *26*, 3894–3901; b) Y. Wang, Y. Di, M. Antonietti, H. R. Li, X. F. Chen, X. C. Wang, *Chem. Mater.* **2010**, *22*, 5119–5121; c) L. G. Zhang, X. F. Chen, J. Guan, Y. J. Jiang, T. G. Hou, X. D. Mu, *MRS Bull.* **2013**, *48*, 3485–3491; d) G. Liu, P. Niu, C. H. Sun, S. C. Smith, Z. G.

Chen, G. Q. Lu, H. M. Cheng, *J. Am. Chem. Soc.* **2010**, *132*, 11642 – 11648.
[17] G. G. Zhang, M. W. Zhang, X. X. Ye, X. Q. Qiu, S. Lin, X. C. Wang, *Adv. Mater.* **2014**, *26*, 805 – 809.
[18] a) X. C. Wang, X. F. Chen, A. Thomas, X. Z. Fu, M. Antonietti, *Adv. Mater.* **2009**, *21*, 1609 – 1612; b) Z. X. Ding, X. F. Chen, M. Antonietti, X. C. Wang, *ChemSusChem* **2011**, *4*, 274 – 281.
[19] S. Z. Hu, L. Ma, J. G. You, F. Y. Li, Z. P. Fan, G. Lu, D. Liu, J. Z. Gui, *Appl. Surf. Sci.* **2014**, *311*, 164 – 171.
[20] G. H. Dong, K. Zhao, L. Z. Zhang, *Chem. Commun.* **2012**, *48*, 6178 – 6180.
[21] J. S. Zhang, X. F. Chen, K. Takanabe, K. Maeda, K. Domen, J. D. Epping, X. Z. Fu, M. Antonietti, X. C. Wang, *Angew. Chem. Int. Ed.* **2010**, *49*, 441 – 444; *Angew. Chem.* **2010**, *122*, 451 – 454.
[22] E. Kroke, M. Schwarz, E. Horath-Bordon, P. Kroll, B. Noll, A. D. Norman, *New J. Chem.* **2002**, *26*, 508 – 512.
[23] J. S. Zhang, G. G. Zhang, X. F. Chen, S. Lin, L. Moehlmann, G. Dolega, G. Lipner, M. Antonietti, S. Blechert, X. C. Wang, *Angew. Chem. Int. Ed.* **2012**, *51*, 3183 – 3187; *Angew. Chem.* **2012**, *124*, 3237 – 3241.
[24] M. W. Zhang, X. C. Wang, *Energy Environ. Sci.* **2014**, *7*, 1902 – 1906.
[25] J. S. Zhang, M. W. Zhang, S. Lin, X. Z. Fu, X. C. Wang, *J. Catal.* **2014**, *310*, 24 – 30.
[26] S. Chu, Y. Wang, Y. Guo, J. Y. Feng, C. C. Wang, W. J. Luo, X. X. Fan, Z. G. Zou, *ACS Catal.* **2013**, *3*, 912 – 919.
[27] Y. Chen, J. S. Zhang, M. W. Zhang, X. C. Wang, *Chem. Sci.* **2013**, *4*, 3244 – 3248.
[28] Y. B. Guo, L. Xu, H. B. Liu, Y. J. Li, C. M. Che, Y. L. Li, *Adv. Mater.* **2015**, *27*, 985 – 1013.
[29] a) M. Osada, T. Sasaki, *Adv. Mater.* **2012**, *24*, 210 – 228; b) J. X. Low, S. W. Cao, J. G. Yu, S. Wageh, *Chem. Commun.* **2014**, *50*, 10768 – 10777.
[30] X. D. Zhang, X. Xie, H. Wang, J. J. Zhang, B. C. Pan, Y. Xie, *J. Am. Chem. Soc.* **2013**, *135*, 18 – 21.
[31] a) H. X. Zhao, H. T. Yu, X. Quan, S. Chen, Y. B. Zhang, H. M. Zhao, H. Wang, *Appl. Catal. B* **2014**, *152*, 46 – 50; b) S. B. Yang, Y. J. Gong, J. S. Zhang, L. Zhan, L. L. Ma, Z. Y. Fang, R. Vajtai, X. C. Wang, P. M. Ajayan, *Adv. Mater.* **2013**, *25*, 2452 – 2456.
[32] X. J. She, H. Xu, Y. G. Xu, J. Yan, J. X. Xia, L. Xu, Y. H. Song, Y. Jiang, Q. Zhang, H. M. Li, *J. Mater. Chem. A* **2014**, *2*, 2563 – 2570.
[33] S. Bai, X. J. Wang, C. Y. Hu, M. L. Xie, J. Jiang, Y. J. Xiong, *Chem. Commun.* **2014**, *50*, 6094 – 6097.
[34] Q. Y. Lin, L. Li, S. J. Liang, M. H. Liu, J. H. Bi, L. Wu, *Appl. Catal. B* **2015**, *163*, 135 – 142.
[35] L. Y. Huang, Y. P. Li, H. Xu, Y. G. Xu, J. X. Xia, K. Wang, H. M. Li, X. N. Cheng, *RSC Adv.* **2013**, *3*, 22269 – 22279.
[36] J. Xu, L. W. Zhang, R. Shi, Y. F. Zhu, *J. Mater. Chem. A* **2013**, *1*, 14766 – 14772.
[37] H. X. Zhao, H. T. Yu, X. Quan, S. Chen, H. M. Zhao, H. Wang, *RSC Adv.* **2014**, *4*, 624 – 628.
[38] Y. Yin, J. C. Han, X. H. Zhang, Y. M. Zhang, J. G. Zhou, D. Muir, R. Sutarto, Z. H. Zhang, S. W. Liu, B. Song, *RSC Adv.* **2014**, *4*, 32690 – 32697.
[39] a) P. Niu, L. L. Zhang, G. Liu, H. M. Cheng, *Adv. Funct. Mater.* **2012**, *22*, 4763 – 4770; b) H. Xu, J. Yan, X. J. She, L. Xu, J. X. Xia, Y. G. Xu, Y. H. Song, L. Y. Huang, H. M. Li, *Nanoscale* **2014**, *6*, 9866 – 9866.
[40] K. Dai, L. H. Lu, Q. Liu, G. P. Zhu, X. Q. Wei, J. Bai, L. L. Xuan, H. Wang, *Dalton Trans.* **2014**, *43*, 6295 – 6299.
[41] Z. W. Tong, D. Yang, T. X. Xiao, Y. Tian, Z. Y. Jiang, *Chem. Eng. J.* **2015**, *260*, 117 – 125.
[42] S. W. Cao, Y. P. Yuan, J. Fang, M. M. Shahjamali, F. Y. C. Boey, J. Barber, S. C. J. Loo, C. Xue, *Int. J. Hydrogen Energy* **2013**, *38*, 1258 – 1266.
[43] Z. Y. Zhang, J. D. Huang, M. Y. Zhang, Q. Yuan, B. Dong, *Appl. Catal. B* **2015**, *163*, 298 – 305.
[44] X. D. Zhuang, Y. Y. Mai, D. Q. Wu, F. Zhang, X. L. Feng, *Adv. Mater.* **2015**, *27*, 403 – 427.
[45] S. Han, D. Q. Wu, S. Li, F. Zhang, X. L. Feng, *Adv. Mater.* **2014**, *26*, 849 – 864.
[46] X. C. Wang, K. Maeda, X. F. Chen, K. Takanabe, K. Domen, Y. D. Hou, X. Z. Fu, M. Antonietti, *J. Am. Chem. Soc.* **2009**, *131*, 1680 – 1681.
[47] J. H. Sun, J. S. Zhang, M. W. Zhang, M. Antonietti, X. Z. Fu, X. C. Wang, *Nat. Commun.* **2012**, *3*, 1139.
[48] a) X. H. Li, J. S. Zhang, X. F. Chen, A. Fischer, A. Thomas, M. Antonietti, X. C. Wang, *Chem. Mater.* **2011**, *23*, 4344 – 4348; b) Y. Zheng, L. H. Lin, X. J. Ye, F. S. Guo, X. C. Wang, *Angew. Chem. Int. Ed.* **2014**, *53*, 11926 – 11930; *Angew. Chem.* **2014**, *126*, 12120 – 12124.
[49] G. F. Jiang, C. H. Zhou, X. Xia, F. Q. Yang, D. S. Tong, W. H. Yu, S. M. Liu, *Mater. Lett.* **2010**, *64*, 2718 – 2721.
[50] a) J. Liu, M. Antonietti, *Energy Environ. Sci.* **2013**, *6*, 1486; b) J. Liu, R. Cazelles, Z. P. Chen, H. Zhou, A. Galarneau, M. Antonietti, *Phys. Chem. Chem. Phys.* **2014**, *16*, 14699 – 14705.
[51] D. D. Zheng, C. J. Huang, X. C. Wang, *Nanoscale* **2015**, *7*, 465 – 470.
[52] Y. Wang, J. S. Zhang, X. C. Wang, M. Antonietti, H. R. Li, *Angew. Chem. Int. Ed.* **2010**, *49*, 3356 – 3359; *Angew. Chem.* **2010**, *122*, 3428 – 3431.
[53] H. J. Yan, *Chem. Commun.* **2012**, *48*, 3430 – 3432.
[54] a) Z. Z. Lin, X. C. Wang, *ChemSusChem* **2014**, *7*, 1547 – 1550; b) Z. Ma, J. H. Yu, S. Dai, *Adv. Mater.* **2010**, *22*, 261 – 285.
[55] J. S. Xu, T. J. K. Brenner, Z. P. Chen, D. Neher, M. Antonietti, M. Shalom, *ACS Appl. Mater. Interfaces* **2014**, *6*, 16481 – 16486.
[56] Y. Ishida, L. Chabanne, M. Antonietti, M. Shalom, *Langmuir* **2014**, *30*, 447 – 451.
[57] M. Shalom, S. Inal, C. Fettkenhauer, D. Neher, M. Antonietti, *J. Am. Chem. Soc.* **2013**, *135*, 7118 – 7121.
[58] a) Y. S. Jun, E. Z. Lee, X. C. Wang, W. H. Hong, G. D. Stucky, A. Thomas, *Adv. Funct. Mater.* **2013**, *23*, 3661 – 3667; b) Y. S. Jun, J. Park, S. U. Lee, A. Thomas, W. H. Hong, G. D. Stucky, *Angew. Chem. Int. Ed.* **2013**, *52*, 11083 – 11087; *Angew. Chem.* **2013**, *125*, 11289 – 11293.
[59] Y. J. Cui, Z. X. Ding, X. Z. Fu, X. C. Wang, *Angew. Chem. Int. Ed.* **2012**, *51*, 11814 – 11818; *Angew. Chem.* **2012**, *124*, 11984 – 11988.
[60] H. Montigaud, B. Tanguy, G. Demazeau, S. Courjault, M. Birot, J. Dunogues, *C. R. Acad. Sci. Ser. IIb* **1997**, *325*, 229 – 234.
[61] G. H. Dong, L. Z. Zhang, *J. Mater. Chem.* **2012**, *22*, 1160 – 1166.
[62] Y. Chen, B. Wang, S. Lin, Y. F. Zhang, X. C. Wang, *J. Phys. Chem. C* **2014**, *118*, 29981 – 29989.
[63] Z. Z. Lin, X. C. Wang, *Angew. Chem. Int. Ed.* **2013**, *52*, 1735 – 1738; *Angew. Chem.* **2013**, *125*, 1779 – 1782.
[64] a) Y. Ham, K. Maeda, D. Cha, K. Takanabe, K. Domen, *Chem. Asian J.* **2013**, *8*, 218 – 224; b) H. L. Gao, S. C. Yan, J. J. Wang, Y. A. Huang, P. Wang, Z. S. Li, Z. G. Zou, *Phys. Chem. Chem. Phys.* **2013**, *15*, 18077 – 18084; c) B. Jürgens, E. Irran, J. Senker, P. Kroll, H. Müller, W. Schnick, *J. Am. Chem. Soc.* **2003**, *125*, 10288 – 10300; d) B. V. Lotsch, M. Döblinger, J. Sehnert, L. Seyfarth, J. Senker, O. Oeckler, W. Schnick, *Chem. Eur. J.* **2007**, *13*, 4969 – 4980.
[65] G. Algara-Siller, N. Severin, S. Y. Chong, T. Björkman, R. G. Palgrave, A. Laybourn, M. Antonietti, Y. Z. Khimyak, A. V. Krasheninnikov, J. P. Rabe, U. Kaiser, A. I. Cooper, A. Thomas, M. J. Bojdys, *Angew. Chem. Int. Ed.* **2014**, *53*, 7450 – 7455; *Angew. Chem.* **2014**, *126*, 7580 – 7585.
[66] S. Y. Chong, J. T. A. Jones, Y. Z. Khimyak, A. I. Cooper, A. Thomas, M. Antonietti, M. J. Bojdys, *J. Mater. Chem. A* **2013**, *1*, 1102 – 1107.
[67] E. J. McDermott, E. Wirnhier, W. Schnick, K. S. Virdi, C. Scheu, Y. Kauffmann, W. D. Kaplan, E. Z. Kurmaev, A. Moewes, *J. Phys. Chem. C* **2013**, *117*, 8806 – 8812.

[68] M. J. Bojdys, N. Severin, J. P. Rabe, A. I. Cooper, A. Thomas, M. Antonietti, *Macromol. Rapid Commun.* **2013**, *34*, 850 – 854.
[69] K. Schwinghammer, M. B. Mesch, V. Duppel, C. Ziegler, J. Senker, B. V. Lotsch, *J. Am. Chem. Soc.* **2014**, *136*, 1730 – 1733.
[70] K. Schwinghammer, B. Tuffy, M. B. Mesch, E. Wirnhier, C. Martineau, F. Taulelle, W. Schnick, J. Senker, B. V. Lotsch, *Angew. Chem. Int. Ed.* **2013**, *52*, 2435 – 2439; *Angew. Chem.* **2013**, *125*, 2495 – 2499.
[71] M. K. Bhunia, K. Yamauchi, K. Takanabe, *Angew. Chem. Int. Ed.* **2014**, *53*, 11001 – 11005; *Angew. Chem.* **2014**, *126*, 11181 – 11185.
[72] C. S. Pan, J. Xu, Y. J. Wang, D. Li, Y. F. Zhu, *Adv. Funct. Mater.* **2012**, *22*, 1518 – 1524.
[73] S. C. Yan, S. B. Lv, Z. S. Li, Z. G. Zou, *Dalton Trans.* **2010**, *39*, 1488 – 1491.
[74] a) Y. D. Hou, A. B. Laursen, J. S. Zhang, G. G. Zhang, Y. S. Zhu, X. C. Wang, S. Dahl, I. Chorkendorff, *Angew. Chem. Int. Ed.* **2013**, *52*, 3621 – 3625; *Angew. Chem.* **2013**, *125*, 3709 – 3713; b) J. D. Hong, Y. S. Wang, Y. B. Wang, W. Zhang, R. Xu, *ChemSusChem* **2013**, *6*, 2263 – 2268; c) S. W. Cao, Y. P. Yuan, J. Barber, S. C. J. Loo, C. Xue, *Appl. Surf. Sci.* **2014**, *319*, 344 – 349.
[75] Q. J. Xiang, J. G. Yu, M. Jaroniec, *J. Phys. Chem. C* **2011**, *115*, 7355 – 7363.
[76] a) J. S. Zhang, M. W. Zhang, R. Q. Sun, X. C. Wang, *Angew. Chem. Int. Ed.* **2012**, *51*, 10145 – 10149; *Angew. Chem.* **2012**, *124*, 10292 – 10296; b) S. W. Zhang, L. P. Zhao, M. Y. Zeng, J. X. Li, J. Z. Xu, X. K. Wang, *Catal. Today* **2014**, *224*, 114 – 121.
[77] a) S. Gawande, S. R. Thakare, *ChemCatChem* **2012**, *4*, 1759 – 1763; b) C. A. Caputo, M. A. Gross, V. W. Lau, C. Cavazza, B. V. Lotsch, E. Reisner, *Angew. Chem. Int. Ed.* **2014**, *53*, 11538 – 11542; *Angew. Chem.* **2014**, *126*, 11722 – 11726; c) G. G. Zhang, S. Zang, X. C. Wang, *ACS Catal.* **2015**, *5*, 941 – 947; d) G. G. Zhang, C. J. Huang, X. C. Wang, *Small* **2015**, *11*, 1215 – 1221.
[78] Y. J. Zhong, Z. Q. Wang, J. Y. Feng, S. C. Yan, H. T. Zhang, Z. S. Li, Z. G. Zou, *Appl. Surf. Sci.* **2014**, *295*, 253 – 259.
[79] D. J. Martin, P. J. T. Reardon, S. J. A. Moniz, J. W. Tang, *J. Am. Chem. Soc.* **2014**, *136*, 12568 – 12571.
[80] a) P. Niu, Y. Yang, J. C. Yu, G. Liu, H. M. Cheng, *Chem. Commun.* **2014**, *50*, 10837 – 10840; b) J. L. Lin, Z. M. Pan, X. C. Wang, *ACS Sustainable Chem. Eng.* **2014**, *2*, 353 – 358; c) R. Kuriki, K. Sekizawa, O. Ishitani, K. Maeda, *Angew. Chem. Int. Ed.* **2015**, *54*, 2406 – 2409; *Angew. Chem.* **2015**, *127*, 2436 – 2439; d) G. G. Zhang, Z. A. Lan, X. C. Wang, *ChemCatChem* **2015**, *7*, 1422 – 1423.
[81] a) C. J. Huang, C. Chen, M. W. Zhang, L. H. Lin, X. X. Ye, S. Lin, M. Antonietti, X. C. Wang, *Nat. Commun.* **2015**, *6*, 7698; b) F. Chang, Y. C. Xie, C. L. Li, J. Chen, J. T. Luo, X. F. Hu, J. W. Shen, *Appl. Surf. Sci.* **2013**, *280*, 967 – 974; c) J. G. Yu, S. H. Wang, J. X. Low, W. Xiao, *Phys. Chem. Chem. Phys.* **2013**, *15*, 16883 – 16890.
[82] J. H. Huang, W. K. Ho, X. C. Wang, *Chem. Commun.* **2014**, *50*, 4338 – 4340.
[83] F. Z. Su, S. C. Mathew, G. Lipner, X. Z. Fu, M. Antonietti, S. Blechert, X. C. Wang, *J. Am. Chem. Soc.* **2010**, *132*, 16299 – 16301.
[84] F. Z. Su, S. C. Mathew, L. Mohlmann, M. Antonietti, X. C. Wang, S. Blechert, *Angew. Chem. Int. Ed.* **2011**, *50*, 657 – 660; *Angew. Chem.* **2011**, *123*, 683 – 686.
[85] X. J. Ye, Y. J. Cui, X. C. Wang, *ChemSusChem* **2014**, *7*, 738 – 742.
[86] J. Liu, J. H. Huang, H. Zhou, M. Antonietti, *ACS Appl. Mater. Interfaces* **2014**, *6*, 8434 – 8440.
[87] a) S. W. Cao, J. X. Low, J. G. Yu, M. Jaroniec, *Adv. Mater.* **2015**, *27*, 2150 – 2176.
[88] S. W. Cao, J. G. Yu, *J. Phys. Chem. Lett.* **2014**, *5*, 2101 – 2107.
[89] D. J. Martin, K. P. Qiu, S. A. Shevlin, A. D. Handoko, X. W. Chen, Z. X. Guo, J. W. Tang, *Angew. Chem. Int. Ed.* **2014**, *53*, 9240 – 9245; *Angew. Chem.* **2014**, *126*, 9394 – 9399.
[90] a) J. S. Zhang, M. W. Zhang, L. H. Lin, X. C. Wang, *Angew. Chem. Int. Ed.* **2015**, *54*, 6297 – 6301; *Angew. Chem.* **2015**, *127*, 6395 – 6399; b) M. Shalom, S. Gimenez, F. Schipper, I. Herraiz-Cardona, J. Bisquert, M. Antonietti, *Angew. Chem. Int. Ed.* **2014**, *53*, 3654 – 3658; *Angew. Chem.* **2014**, *126*, 3728 – 3732; c) J. S. Xu, T. J. K. Brenner, L. Chabanne, D. Neher, M. Antonietti, M. Shalom, *J. Am. Chem. Soc.* **2014**, *136*, 13486 – 13489.
[91] a) J. S. Zhang, X. C. Wang, *Angew. Chem. Int. Ed.* **2015**, *54*, 7230 – 7232; *Angew. Chem.* **2015**, *127*, 7336 – 7338; b) C. Pan, T. Takata, M. Nakabayashi, T. Matsumoto, N. Shibata, Y. Ikuhara, K. Domen, *Angew. Chem. Int. Ed.* **2015**, *54*, 2955 – 2959; *Angew. Chem.* **2015**, *127*, 2998 – 3002.

Received: February 24, 2015
Published online: October 1, 2015